**Title**
A STUDY OF THE ANTIPROTON ANNIHILATION PROCESS IN COMPLEX NUCLEI



**Author**
Kalogeropoulos, Theodore E.

**Publication Date**
1959-03-06

UCRL 8677

UNIVERSITY OF
CALIFORNIA
*Ernest O. Lawrence*
*Radiation Laboratory*

# A STUDY OF THE ANTIPROTON ANNIHILATION PROCESS IN COMPLEX NUCLEI

## DISCLAIMER

UCRL-8677
Physics and
Mathematics

UNIVERSITY OF CALIFORNIA
Lawrence Radiation Laboratory
Berkeley, California

Contract No. W-7405-eng-48

# A STUDY OF THE ANTIPROTON ANNIHILATION PROCESS IN COMPLEX NUCLEI

Theodore E. Kalogeropoulos
(Thesis)

March 6, 1959

Printed for the U. S. Atomic Energy Commission

Printed in USA. Price $1.75. Available from the
Office of Technical Services
U.S. Department of Commerce
Washington 25, D. C.

# A STUDY OF THE ANTIPROTON ANNIHILATION PROCESS IN COMPLEX NUCLEI

## Table of Contents

# A STUDY OF THE ANTIPROTON ANNIHILATION PROCESS IN COMPLEX NUCLEI

Theodore E. Kalogeropoulos

Lawrence Radiation Laboratory
University of California
Berkeley, California

March 6, 1959

## ABSTRACT

The antiproton annihilation process in complex nuclei has been further studied in photographic emulsions. When a 19.8 gr/cm$^2$ LiH absorber was introduced in an existing antiproton beam, the antiproton-to-meson ratio improved by a factor of about 10, becoming 1/50,000. Thus in a single stack exposed to this improved beam, 165 antiprotons were found. These together with 20 more found in other stacks and the 36 reported in the "Antiproton Collaboration Experiment" (a total of 221 analysed stars) are included in this analysis.

From this analysis the annihilation process in complex nuclei can be interpreted to proceed as follows: The antiproton annihilates itself with one nucleon (proton or neutron), transforming all the available energy mainly into $\pi$ mesons of average multiplicity $5.36 \pm 0.28$ with an occasional K-$\overline{K}$ emission of frequency $(3.5 \pm 1.5\%)$ per star. The mesons interact with the nucleus leaving it in an excited state. The nucleus releases the excitation energy through nucleon emission. On the average, the stars in flight have more excitation than those at rest.

By the use of this experimental data and available information on pion interactions in nuclear matter, the fraction of interacting pions (absorbed and inelastically scattered) has been deduced for the stars in flight and at rest separately. Furthermore, it is shown that with a better knowledge of the pion interactions in nuclear matter, we can use antiproton annihilations to investigate the nucleon distribution at the surface

of the nucleus.

The pion-pion angular distribution has been deduced on the basis of energy-momentum conservation, by the use of the Fermi statistical model of the annihilation with Lorentz-invariant phase space. The theoretical distribution agrees with the experimental one if an adjustment of the interaction volume is made to account for the observed pion multiplicity. A strong pion-pion interaction is thus unlikely.

# I. INTRODUCTION

The success of the Dirac Theory of the electron in predicting its charge conjugate, the positron, stimulated the interest of the experimental physicist to search for the charge conjugate of the proton, the antiproton. The differences and the similarities between proton and antiproton required by the theory are summarized in Table I, which indicates also the properties verified by the first experiments.

Table I

| Property | Proton | Antiproton | Exper. verified by: |
|---|---|---|---|
| Charge | +e | -e | Counters (sign and magnitude)[1] Emulsions (magnitude)[2] |
| Mass | m | m | Counters[1] emulsions[2] |
| Spin | 1/2 | 1/2 | |
| Magnetic moment | $\mu$ | $-\mu$ | |
| Mean life time | $\tau$ | $\tau$ | $\tau_{\overline{P}}$ larger than $10^{-7}$ sec[1, 2] |
| Creation in pairs | | | Counters[1] (from excitation function) |
| Annihilation | | | Emulsions[2] and counters[1] |
| I-Spin T | 1/2 | 1/2 | |
| $T_3$ | 1/2 | -1/2 | |
| Parity | + | - | |

Immediately after a beam of protons with energy above the threshold (~5.8 Bev) for antiproton production was available at the Berkeley Bevatron, a search for the antiproton started with scintillation counters. In the fall of 1955 the antiproton was discovered by Chamberlain, Segrè, Wiegand, and Ypsilantis.[1] Charge, mass, and stability against spontaneous decay were the verified properties.

At about the same time, emulsion groups in Berkeley and Rome were undertaking an intensive search for antiprotons in photographic emulsions exposed at the Bevatron. Except for the sign of the charge, the emulsion work verified the counter experiment; in addition, the annihilation property was observed. A total of 36 antiprotons were found; these were reported in the "Antiproton Collaboration Experiment",[2] thereafter cited as ACE.

Both experiments established rather conclusively the existence of the antiproton. The research then was directed toward the investigation of the properties of interaction of antiprotons with matter and the investigation of the modes of annihilation with improved statistics.

In order to continue this work, it was necessary to improve the antiproton beam, increasing the ratio of antiprotons to other spurious particles (mainly pions, muons, and electrons). A successful step was taken in this direction, when a LiH absorber was introduced in the beam, thus producing a momentum difference between antiprotons and mesons which was resolved later into a spatial separation by momentum-analysing magnets. In a stack exposed to this beam, 165 antiprotons were found. The analysis of these stars combined with the 36 from ACE and the 20 others found in other stacks has been reported.[3,4]

The present work is rather a supplement to that work, and from the experimental point of view does not offer anything new. It is intended to be an extension of the previous analysis and a further interpretation of the experimental results. In order to present this work in some organic form, the experiment and those experimental results connected with the discussion and analysis will be presented briefly.

## II. EXPERIMENTAL PROCEDURE

### A. The Separated Antiproton Beam.

In Fig. 1 the experimental arrangement of the separated antiproton beam is shown. The spectrograph is the same one used in a previous counter experiment[5] with the addition of the LiH absorber and the magnet $M_c$. A carbon target at T is bombarded by the circulating proton beam of the Bevatron at the end of each accelerating cycle. A fraction of the particles coming out of the target, deflected by the fringing magnetic field of the Bevatron, enters the spectrograph. These particles contain about one antiproton per million other particles.

The system of the quadrupole magnet $Q_1$ together with the analyzing magnet $M_1$ focuses the negative particles of momentum $819 \pm 4\%$-Mev/c at $F_1$. Quadrupole magnet L plays a role similar to a field lens correcting lateral momentum aberration.

In order to achieve a separation in momentum depending on the mass, a wedge-shaped LiH absorber of medium thickness 19.8 gr/cm$^2$ has been placed at $F_1$. The beam is expected to have 700-Mev/c and 777-Mev/c momentum for antiprotons and light mesons respectively after it has passed through the absorber. Because of the shape of the absorber, the original spread in momentum (4%) is preserved.

The momentum difference achieved between the antiprotons and the light mesons is resolved into a spatial separation by the subsequent system of magnets at $F_2$. The magnet $M_c$ serves two purposes: (a) it deflects the particles according to momentum and thus further increases the spatial separation between antiprotons and mesons; and (b) it clears from the beam the highly unwanted protons (produced by pion interactions) which can be confused with the antiprotons.

At $F_2$ a stack of 200 Ilford-$G_5$ emulsions (15 cm by 23 cm by 600 $\mu$) was exposed for a total integrated beam of $4 \times 10^{13}$ protons on the target. In this stack (No. 78), 165 antiprotons were found constituting the majority of the antiprotons studied in this work. In this beam a ratio of antiprotons to minimum ionizing particles of 1/50,000 has been obtained, showing an improvement over the previous beam by a factor of ten.

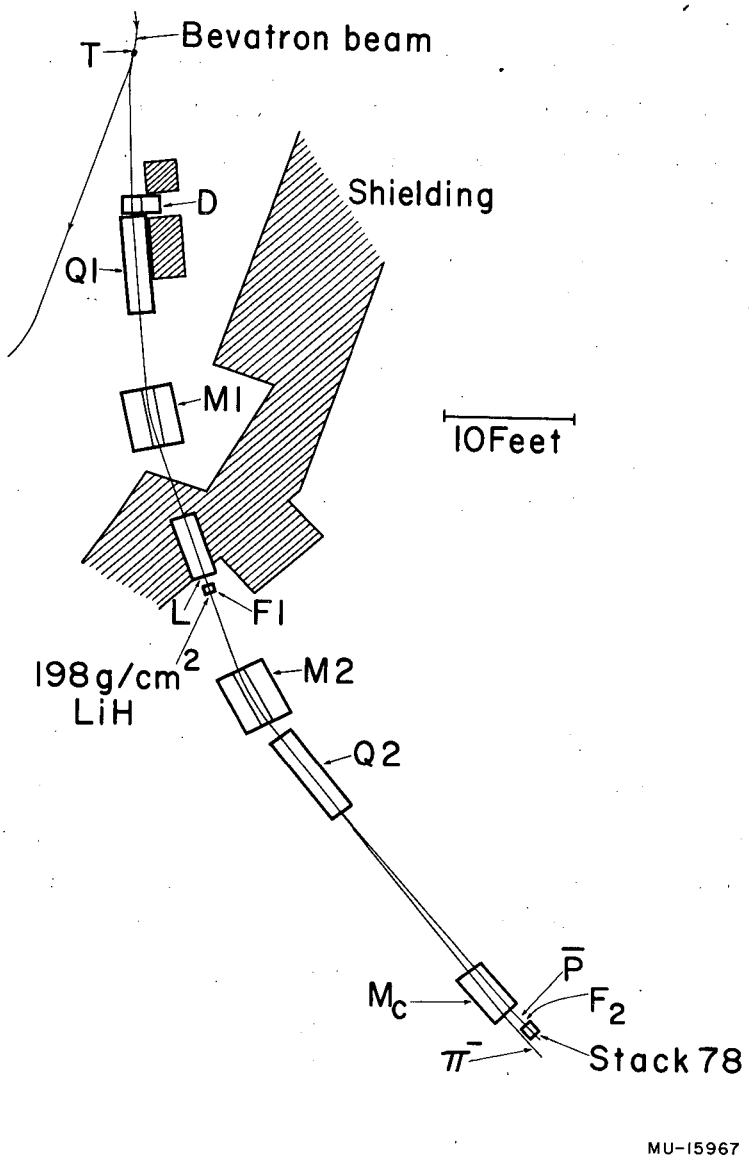


Fig. 1. The exposure geometry.

In Fig. 2 the antiprotons coming to rest have been plotted as a function of their range (R) in emulsion and their horizontal linear coordinate Y which is perpendicular to the beam. A linear fit to this distribution is also shown by the line $\overline{R}$ (Y). The dependence between $\overline{R}$ and Y is the result of the analysing magnet $M_c$ and the momentum spread in the beam.

From measurements of the density of $\pi^-$ stars in the stack, a 4% $\pi^-$ contamination was found. Measurements of the intensity of the beam along the beam (Fig. 3) revealed the electron component. The position of the maximum and the relative increase of the intensity due to electron multiplication require a 48% contamination in electrons. The rest of the particles (48%) were assumed to be muons. We see that in the antiproton separated beam most of the pions were removed, while a large number of muons and electrons remained.

## B. Scanning and Proton Contamination.

The emulsion plates were scanned under 22x to 53x objectives in combination with 10x eyepieces. The scanning proceeded parallel to the leading edge of the stack, along the Y coordinate, and 5mm away from the edge. The good collimation of the beam has allowed us visually to distinguish the antiprotons from the large background of minimum particles by means of ionization and the angle between the track and the main direction of the beam.

All tracks with ionization about twice minimum and making an angle with the direction of the beam of less than about $10^o$ were considered as antiproton candidates, and they were followed until they either interacted in flight or came to rest. A star usually resulted at the end of these tracks.

Tracks of protonic mass and which produced a star upon coming to rest are certainly antiprotons. A number of particles of protonic mass, however, came to rest without giving any energy release. These tracks, called $P_\rho$, might be protons or antiprotons which either did not annihilate[6] or in which the final products of the annihilation were all neutrals ($\overline{P}_\rho$).

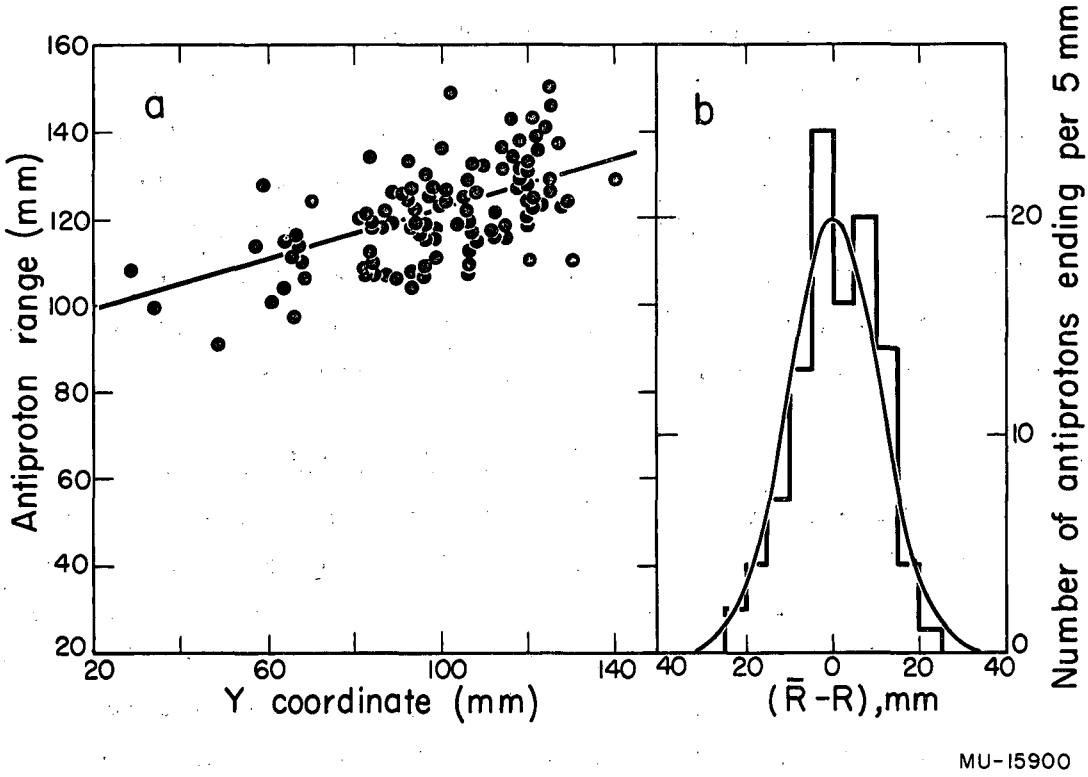


Fig. 2. (a) The range of stopping antiprotons is plotted as a function of the entrace y coordinate. The curve gives the mean antiproton range, $\bar{R}$ as a function of the y coordinate. The momentum dispersion is due to the clearing magnet $M_C$ (see Fig. 13).

(b) The spread in range around $\bar{R}$ as given by the curve in A. The half width at half maximum is about 13 mm. $\Delta R/R$ is thus $\pm$ 0.11, which corresponds to a momentum spread of $\Delta P/P$ equal to $\pm$ 0.029.

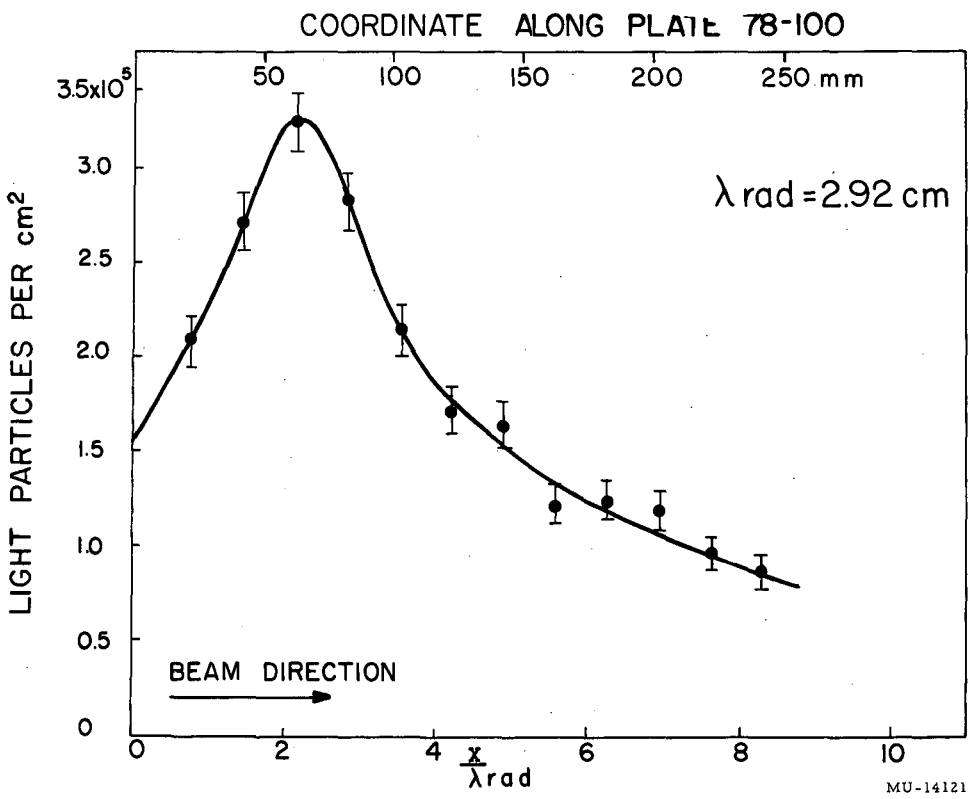


Fig. 3. The transition curve for the light-particle flux. The light-particle flux was measured along the beam direction (the X coordinate along Plate 78-100). The curve is plotted against distance along the plate as measured in radiation lengths in emulsion. The peak at about 2 units of radiation length clearly indicates the presence of a large fraction of electrons in the beam ( ~50 %).

The good collimation of the beam makes possible further examination of the $P_\rho$'s. In Fig. 4 all tracks followed and coming to rest are plotted as a function of $|\bar{R}-R|$ (Fig. 2) and the relative entrance space angle $\theta_{rel}$. The antiprotons are concentrated in a small region close to the origin of the coordinates, while the $P_\rho$'s are statistically uniformally distributed over a larger region. It is then obvious that the particles outside the rectangle ( $|\bar{R}-R| < 2.4$ cm, $\theta_{rel} < 3^o$) containing all the definite antiprotons are accidental protons. We estimate from the density of protons outside the rectangle that $4 \pm 0.7$ protons are present inside the rectangle. There are 7 $P_\rho$ events, two of which occur near the surface of the plates, and possible minimum prongs might have been missed. Comparing those two numbers an estimate of $2\ ^{+3}_{-2}$ % contamination in $\bar{P}_\rho$ stars is obtained. The errors are statistical ones and do not take into account either that some bias is present against picking up tracks with large $\theta_{rel}$ or large $|\bar{R}-R|$ or the possibility that the two tracks near the surface might have a minimum prong. Both of these effects tend to decrease the $2\ ^{+3}_{-2}$ % estimate.

All particles of protonic mass and with $\theta < 3^o$ interacting in flight have resulted in a star. Only three of them have no pions, and the total visible energy release is less than the kinetic energy of the incoming particle. These three stars could be due to proton interactions, $\bar{P}$ charge exchange, or $\bar{P}$ annihilations with the energy given to neutral particles. From the P contamination with $\theta_{rel} < 3^o$ and the proton mean free path for interaction in emulsion, we estimate about 3 proton interactions to be among the antiproton stars in flight. By the use of a 4 mb $\bar{P}$ charge-exchange cross section,[7] we expect 0.5 such events. From these estimates we deduce $2 \pm 1$ stars to be among the 95 stars in flight, which is a very insignificant amount to give any noticeable bias to the analysis.

## C. Measurements on the Prongs.

We used various measuring techniques for the prongs from the annihilation stars depending on the ionization and the dip angle. Projected- and dip-angle measurements have been made for all prongs. For $g/g_0 < 1.3$, grain count measurements were made on all tracks,

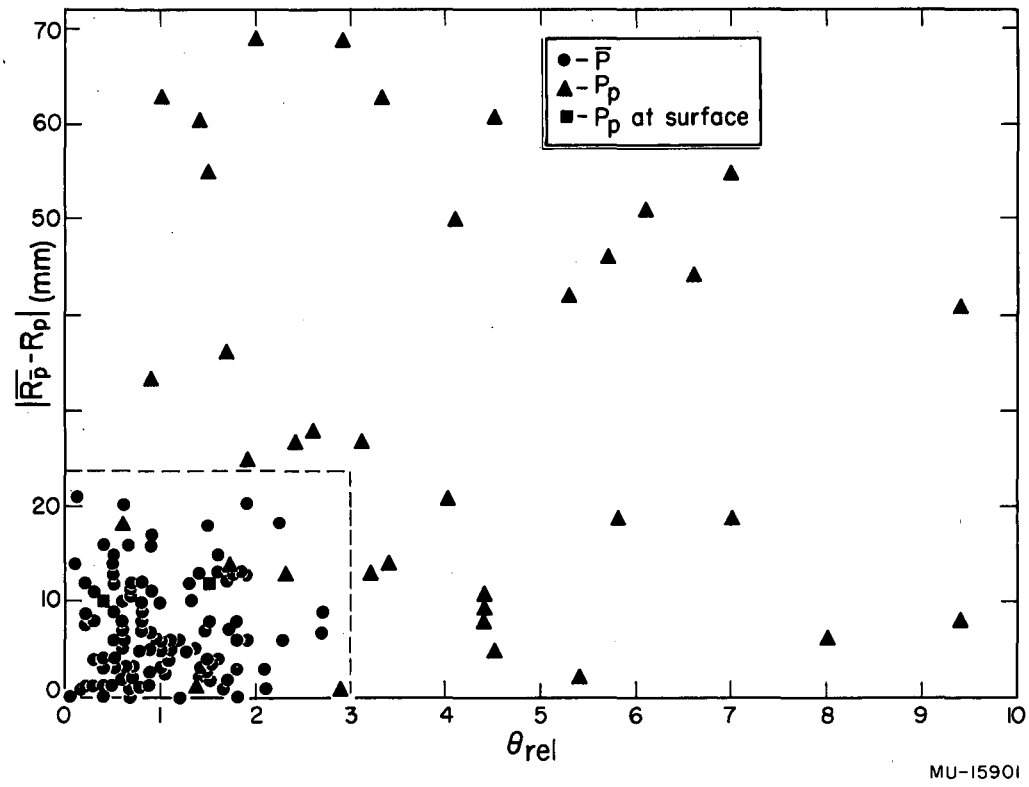


**Fig. 4.** A plot of the deviation in range from the mean range $\Delta R = |\bar{R} - R|$, for ending tracks of protonic mass versus the relative entrance angle $\theta_{rel}$ (space angle). The rectangle determined by $\theta_{rel} \leq 3^{o}$ and $\Delta R \leq 24$mm contains all the identified antiproton tracks.

whereas $p\beta$ measurements using third-difference methods[8] (when needed) have been made for tracks with dip angle $\leq 20^{\circ}$. Except for one energetic electron pair, all these prongs with dip angle $\leq 20^{\circ}$ were light mesons, considered as pions (see Section III, A, 3 ). We have considered all the steeper prongs as pions also. All the prongs were followed for a sufficient length to eliminate low-energy electrons ( ~10 Mev). For $g/g \geq 1.3$ all prongs were followed, and identification and energy measurements were made by standard emulsion techniques. The end points of all prongs ending in the emulsion stack were examined carefully for possible decay secondaries. No attempt was made to distinguish alphas, deuterons, and tritons from protons for ranges $R_H \leq 1$ cm. For $R_H > 1$ cm and angle $\leq 40^{\circ}$, opacity measurements were made. These measurements identified one deuteron, and one particle was either a deuteron or a $\Sigma$ particle.

# III. THE PRODUCTS FROM THE ANNIHILATION STARS

## A. Pions

### 1. The Charged-Pion Multiplicity

In Fig. 5 the distribution of stars as a function of the observed-pion multiplicity is shown separately for stars at rest and in flight. No corrections have been made for the possible presence of $\overline{P}_\rho$ events in the stars at rest or proton contamination and antiproton charge-exchange events in the stars in flight. All these corrections--if any--are very small and can be neglected. From these distributions the following average values per star for the charged-pion multiplicities are obtained: $\langle N_{\pi^\pm} \rangle_{\text{flight}} = 2.50 \pm 0.26$, $\langle N_{\pi^\pm} \rangle_{\text{rest}} = 2.30 \pm 0.28$, and $\langle N_{\pi^\pm} \rangle_{\text{combined}} = 2.41 \pm 0.19$, where the errors represent the statistical standard deviations.

If the annihilation of the antiproton occurs with one kind of nucleon, proton or neutron, then in order to conserve the charge, only modes of annihilation with even or odd numbers of charged pions are respectively allowed. The observed distribution of stars in charged-pion multiplicity is continuous, indicating that antiprotons annihilate with protons as well as with neutrons. We must, however, be overcautious in this statement, because pion-absorption and pion-detection inefficiency reduce any discontinuity in the distribution.

### 2. The Pion Spectrum

In Fig. 6 the measured pion spectrum of the annihilation process in complex nuclei is shown for the stars at rest, in flight, and combined. Although the energy of all pions observed with dip angle $|\beta| \leq 20^\circ$ has been measured, only the pions with $|\beta| \leq 15^\circ$ are included in this spectrum. This low cut-off angle is necessary in order to reduce the systematic errors, due to the distortion of the plates, of the energy measured by the scattering technique. A comparison of the average pion energy as a function of the dip angle showed a systematic decrease, even though the method of third differences was applied to eliminate second-order distortion effects.[8]

Assuming that at very low dip-angles no effects of distortion are present and considering the dependence of the average pion energy

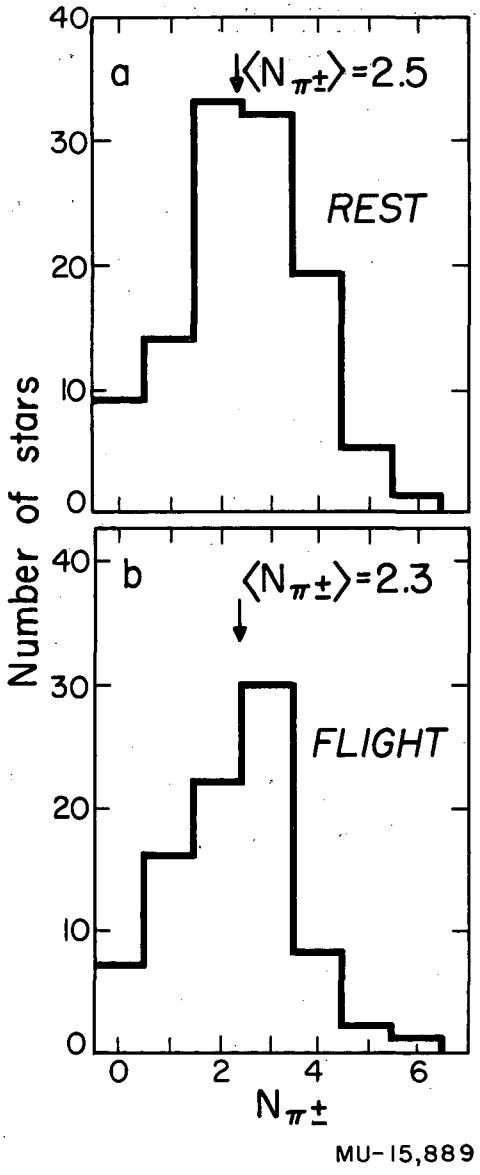


Fig. 5. The observed charged-pion multiplicity distribution from antiproton stars.

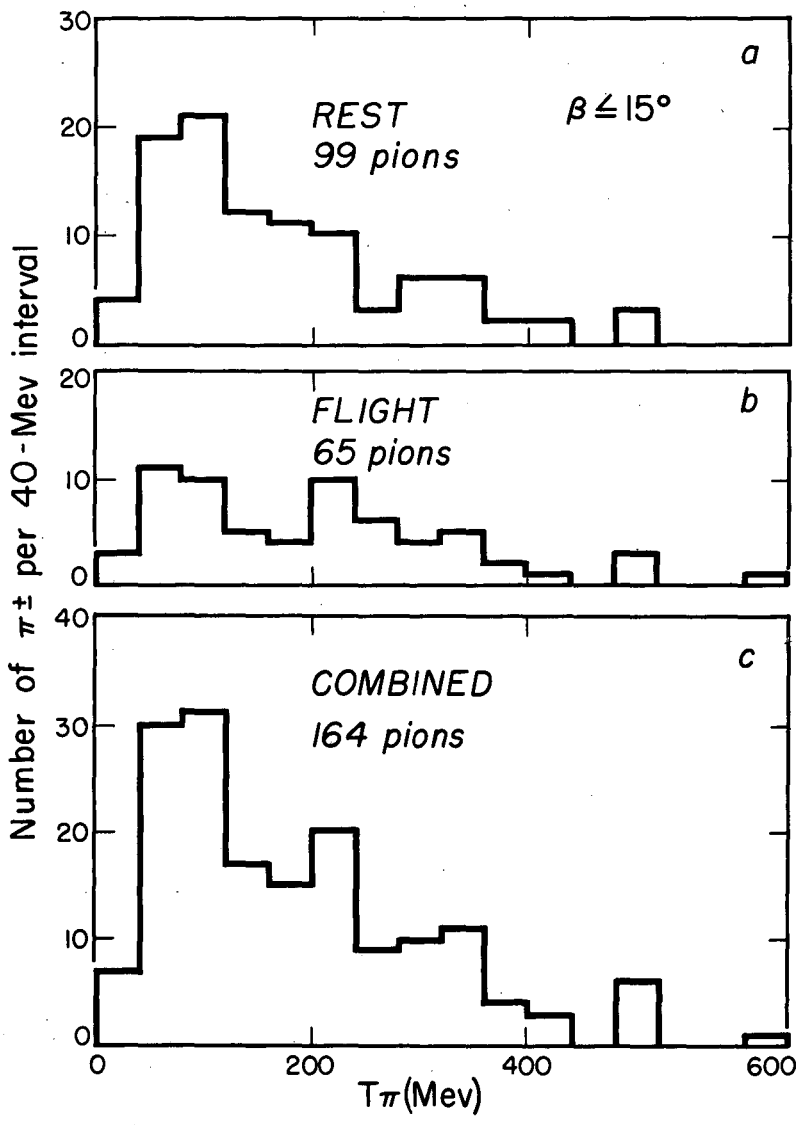


**Fig. 6.** The observed charged-pion spectrum from antiproton stars. Energy measurements included here come from pions with dip angle $< 15^{\circ}$. This represents ~1/4 of the total solid angle.

on the dip angle, we have applied a correction $w_1 = 10 \pm 5$ Mev to the measured average pion energy to account for distortion effects. This correction, however, cannot be reliable, and systematic errors might still be present, thus giving a lower pion energy.

The pion detection efficiency depends on the ionization, and therefore, on the pion energy. Assuming that the efficiency is 100% for ionization $g/g_0 \geq 1.2$, uniform for $g/g_0 < 1.2$, and 90% for all pions, we have deduced a correction $w_2 = 7 \pm 2$ Mev which must be applied to the measured average pion energy to account for this effect.

In Table II the average (measured and corrected) pion energy as a function of the charged-pion multiplicity $N_{\pi^\pm}$, and for stars at rest, in flight, and combined are given. There is also given the expected average pion energy from the normalized Fermi model, (see IV C, 1).

3. The $\pi^+/\pi^-$ Ratio

In photographic emulsions the sign of the charge of a particle can not be determined unless a characteristic of the charge reaction is observed. The pions, coming to rest, reveal their charge. The positive ones, being repulsed by the Coulomb field of the nucleus, decay away from the nucleus, giving a $\mu$ meson of a given range ($\sim 600\mu$). This subsequently comes to rest and decays into a visible electron. On the other hand, the negative pions, being attracted by the nucleus, are captured into Bohr orbits, and because of their large time of decay relative to the transition probabilities from one orbit to the next,[9] they fall into the nuclear field and interact. Thus, from the $\pi^-$ endings, we expect to see either nuclear prongs ($\sigma$ star) or nothing at all ($\rho$ endings) when the energy is given to neutral prongs.

Of all light mesons followed, 76 came to rest, with 22 showing the characteristic of the $\pi^+$ ($\pi^+ \rightarrow \mu^+ \rightarrow e^+$) decay, while 53 produced a $\sigma$ star or a $\rho$ ending characteristic of the $\pi^-$. There was only one case where the charge could not be determined. These 76 meson endings compared with other experimental data on $\pi^+$, $\pi^-$ endings and mass measurements through $g/g_0$-versus-range curves have established that no $\mu$ mesons are present among those light mesons.[4]

Table II

Ratio $\gamma$ of the number of pion-pion angles greater than $90^{\circ}$ to those smaller than $90^{\circ}$, and the average pion-pion angle $\langle\theta\rangle$, as a function of charged pion multiplicity.

| $N_{\pi^{\pm}}$ | At rest | | | In flight | | | Combined | | |
|---|---|---|---|---|---|---|---|---|---|
| | No. of pairs | $\gamma$ | $\langle\theta\rangle$ | No. of pairs | $\gamma$ | $\langle\theta\rangle$ | No. of pairs | $\gamma$ | $\langle\theta\rangle$ |
| 2 | 35 | 1.19 | 90 | 16 | 1.89 | 100 | 51 | 1.44 | 94.2 |
| 3 | 103 | 1.13 | 94 | 84 | 1.90 | 98 | 187 | 1.41 | 95.8 |
| 4 | 114 | 1.59 | 97 | 48 | 1.53 | 99 | 162 | 1.57 | 98.1 |
| 5 | 50 | 1.50 | 101 | 30 | 1.50 | 97 | 80 | 1.50 | 99.6 |
| 6 | 15 | 1.14 | 86 | 15 | 0.88 | 94 | 30 | 1.00 | 89.8 |
| 2-6 | 317 | 1.34 | 95.5 | 193 | 1.64 | 97.7 | 510 | 1.45 | 96.6 |
| | | ±15 | ±5.4 | | ±.24 | ±6.9 | | ±.13 | ±4.3 |

In Fig. 7 the spectra of the $\pi^+$- and $\pi^-$ mesons are shown. The Coulomb barrier of the nucleus, where the annihilation takes place, prevents emission of $\pi^+$ of low energy. For this reason, to find a $\pi^+/\pi^-$ ratio, independent of the Coulomb field, only pions with $T_\pi \geq 20$ Mev have been considered. These pions give a $(\pi^+/\pi^-)_{obs} = 20/44 = 0.45 \pm 0.12$.

The large abundance of $\pi^-$ relative to $\pi^+$ mesons has been interpreted as a combined result of (a) the charge conservation in the annihilation process and (b) the differences in scattering of two types of pions by the nucleus. Assuming charge independence, charge conservation, and that the ratio of annihilations with neutrons to those with protons is the same as the n/p ratio in the emulsion nuclei, we expect a ratio $(\pi^+/\pi^-) = 0.76$. Taking into account also the fact that $\pi^-$ mesons scatter more than $\pi^+$ and that the spectrum of the $\pi^-$ peaks at lower energy than the $\pi^+$ we estimate an over-all ratio $(\pi^+/\pi^-)_{est.} = 0.58$.[4] With all uncertainties involved in this estimate, we might say that the agreement with the observed ratio is satisfactory.

## 4. Antiproton-Pion Angular Distribution

In Fig. 8 the angular distribution between the pions and also the direction of the incoming antiproton for stars at rest and in flight is shown. For the stars at rest an isotropic distribution is expected, while for those in flight a small forward preference is expected by the conservation of momentum. The agreement between the expected and the observed distribution for the stars in flight is indicative of very small scattering, because the scattering tends to reduce any anisotropy. In addition, it can be concluded from these distributions that to a good approximation the pions can be considered to be emitted isotropically in the laboratory system.

## 5. The Experimental Pion-Pion Angular Distribution

From dip- and projected-angle measurements performed on all charged mesons, the angle $\theta$ between each pion pair in every star has been computed. For a star of $N_\pi \pm$ observed charged-pion multiplicity, $N_\pi \pm (N_\pi \pm -1)/2$ pion pairs are possible. Neutral pions,

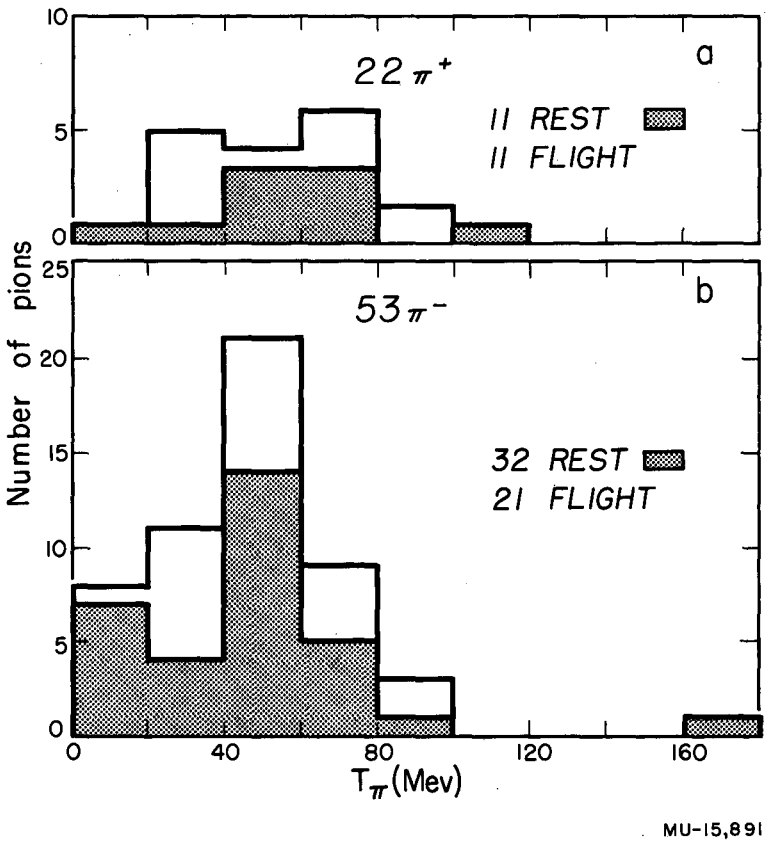


Fig. 7. The energy distribution of pions with identified sign from antiproton stars. The shaded histograms represent pions from antiproton stars at rest.

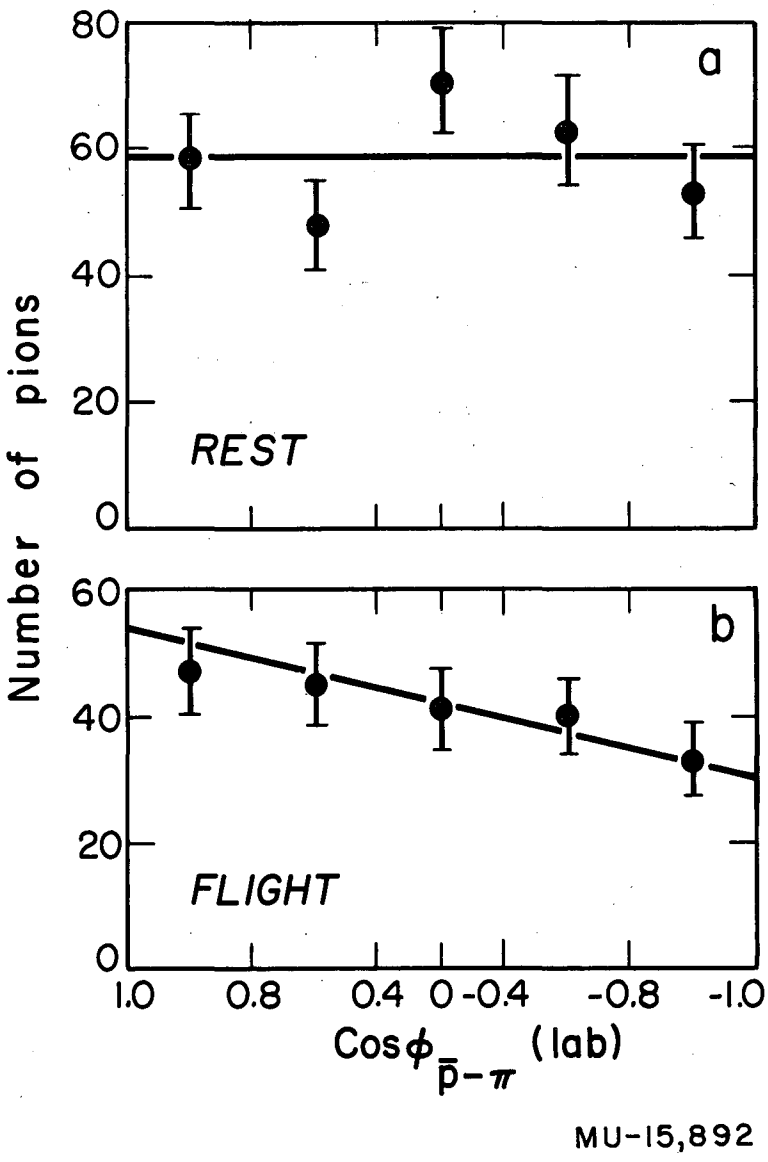


Fig. 8. The pion-emission angles relative to the antiproton direction in the laboratory system. The figure shows the number of pions plotted against the cosine of the emission angle. For the stars at rest, the line corresponding to isotropic emission is shown. For the stars in flight the line corresponding to isotropic emission in the c.m. system suitably averaged over antiproton and pion energies is shown.

and an average of 0.8 charged pions per star have not been observed because of pion absorption and inefficiency in the pion detection. We also note that the observed distribution has been influenced somewhat by the pion scattering inside the nucleus.

The distribution of all charged pion pairs plotted against cos $\theta$ is shown in Fig. 9. This distribution has been examined for stars at rest, in flight, and as a function of $N_{\pi}\pm$. All these subgroups have the same features, and we thus represent all of them combined. In order to give an idea of their similarities, however, the average $\langle\theta\rangle$ and the ratio $\gamma$ of the number of pairs with $\theta \geq 90^{o}$ to those with $\theta < 90^{o}$ for all cases examined are given in Table II. From the experimental distribution a preference of pion pairs toward large angles is characteristic of the distribution. An interpretation of the anisotropy based on the conservation of energy and momentum is discussed in Section IV C, 2, and the theoretical distribution thus obtained is plotted together with the experimental one.

## B. Strange Particles

### 1. K Mesons

The conservation of strangeness and energy demands that the modes of annihilation with no K's or a K-$\bar{K}$ pair be allowed only, and, furthermore, a lower limit in the ionization is set for the K mesons: $g/g_0 \geq 1.2$. All prongs with ionization larger than $1.2g_0$ (where $g_0$ is the ionization of minimum-ionizing particles) were followed, and they either left the stack or came to rest. A few of them interacted in flight. A careful examination of the endings for possible decay prongs has been made. Pions coming to rest are easily distinguished from heavier particles because of their large scattering and their "greyness" close to their ending. In addition, $g/g_0$-vs-range measurements have made possible a definite identification of these particles. Among all prongs followed, only one case of a K meson coming to rest (Star 3-25) has been observed.

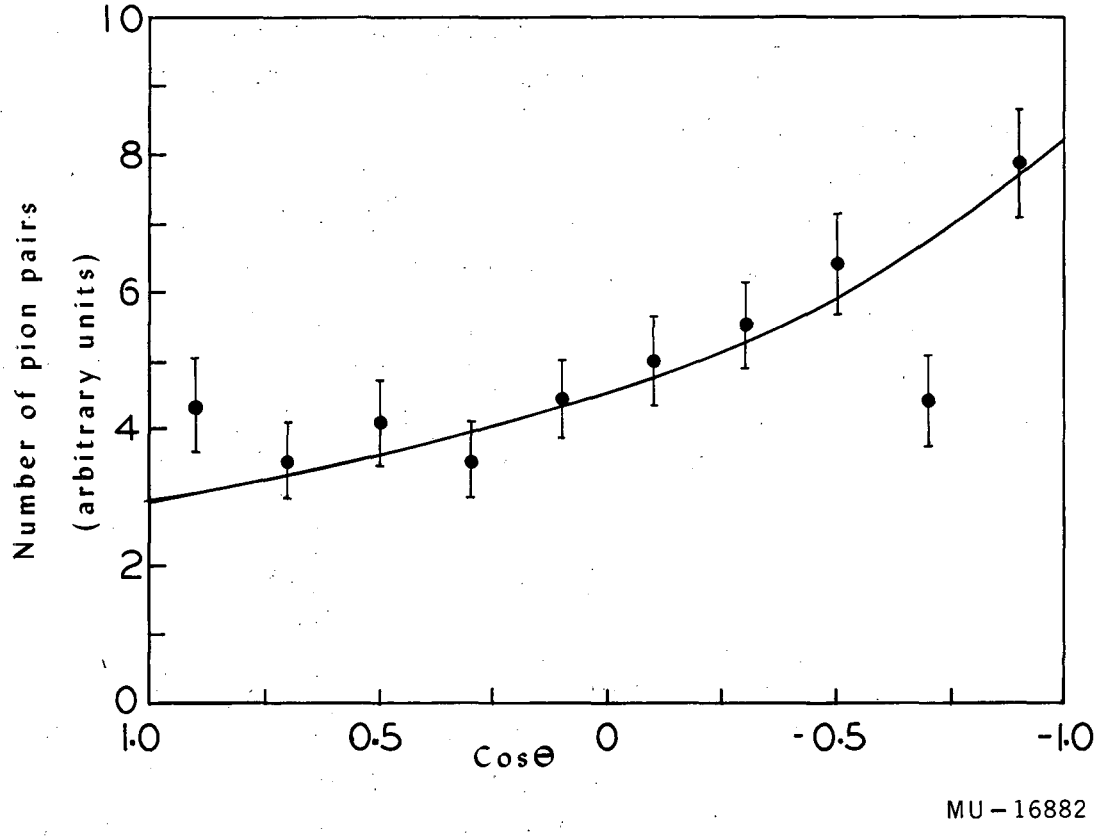


Fig. 9. Distribution of angles between all pion pairs from the antiproton-annihilation stars. The curve corresponds to the distribution expected from energy and momentum conservation.

Since the only way to create a K meson from an annihilation star is by direct production from the annihilation process, this definite example of a K meson proves that they are being produced in the annihilation process.

It is more difficult, however, to identify the prongs which do not end in the emulsion. The most important method of identification used was ionization versus $p\beta c$ measurements by scattering. The distinction between pions and heavier particles was rather easily done, but the distinction among K's and protons is poor due to the distortion of the plates and the small scattering signal. This method becomes very unreliable as the dip angle increases. With all care and refinement of the technique it was possible to identify some of these particles up to $30^{o}$ dip angle.[8] Other standard emulsion techniques (especially scattering measurements with the surface-angles method[2] have been tried above $30^{o}$ dip.

In Table III we summarize all the available information in the K mesons. From this table we can establish lower and upper limits in the K-meson abundance, considering the known and suspected K mesons below $30^{o}$ dip and correcting for the solid angle. For the lower limit we have considered the three definite K's, while for the upper limit all five possible K's have been considered. In order to find the percentage of stars with a $K\text{-}\bar{K}$ pair, corrections have to be made for (a) the $K^{0}\text{-}\bar{K}^{0}$ mode which accounts for about 16% of all stars with K's and (b) the $K^{0}$ - K mode in which the $K^{-}$ has been absorbed by the nucleus and which is estimated to include ~8% of all stars with K's. We thus obtain an estimate of $3.5 \pm 1.5\%$ of the annihilations containing a $K\text{-}\bar{K}$ pair.

From the estimate of the K - $\bar{K}$ abundance and the average energy of the K mesons, $\langle E_{K} \rangle$ = 650 Mev, an estimated average energy per star $\langle \Sigma E_{K\text{-}K^{\pm}} \rangle = 50 \pm 25$ Mev is given to K - meson production.

2. Hyperons (Y)

It is possible that in the annihilation of an antiproton in complex nuclei a hyperon may be produced. This can be explained in two ways: (a) K interaction with the nucleus can result in a hyperon through the

Table III

Data on K mesons (including ambiguous cases) from antiproton stars

| Event no. | Prong no. | Dip angle (degrees) | Available path (cm) | $T_K$ (Mev) | Terminal behavior | Comments |
|---|---|---|---|---|---|---|
| 3-3 | 8 | 15 | 2.47 | 80 | disappears in flight | definite K[a] |
| 3-25 | 1 | 30 | 5.3 | 104 | decays at rest | definite K see Appendix V |
| 3S-59 | 2 | 29 | 8.3 | 235 | leaves stack | definite K |
| 3S-83 | 5 | 23 | 4 | 355 | leaves stack | uncertain identification |
| 3-7 | 3 | 19 | 3.5 | 260 | leaves stack | uncertain identification[a] |
| 2-3 | 2 | 44 | 1.9 | 175 | leaves stack | uncertain steep[a] |
| 3S-3 | 3 | 74 | 7.8 | 120 | comes to rest; nothing at end | uncertain steep |
| 3S-71 | 3 | 67 | 1.5 | 102 | star in flight | uncertain steep |
| 3S-86 | 3 | 64 | 1.7 | 195 | star in flight | uncertain steep |
| 3-3 | 11 | 74 | 4.0 | 195 | leaves stack | uncertain steep[a] |

[a] From Ref. 2.

reaction $K^- + n \rightarrow Y + \pi$, or (b) the annihilation can take place in the presence of a second nucleon according to $\bar{P} + n + n \rightarrow Y + K + n$. In this work an energetic $\Sigma^+$ ($T_{\Sigma^+} = 250$ Mev) is suspected, and a similar case has been reported in ACE.[2] However, hyperons coming from antiproton annihilation stars have definitely been observed in the propane bubble chamber.[10]

## C. Nucleons

### 1. Charged Prongs.

A large fraction of the prongs in the annihilation stars are protons, deuterons, alphas, and more complicated nuclear fragments (recoils). The majority of these prongs have a rather short range, and thus they end in the stack, while the remaining ones leave the stack. We classified these into two categories according to their energy. Evaporation prongs (EV) are the ones with $T_H \lesssim 30$ Mev, and knock-ons (KO) are those with $T_H \gtrsim 30$ Mev.

The evaporation prongs were assumed at first to be protons, and from the range the energy was found. Although many other particles are expected to be present (e.g. deuterons and alphas), this assumption does not appreciably influence the total average energy given to the evaporation prongs per star $\langle \Sigma E_{EV} \rangle$. This can be seen if one considers the difference in energy from range-energy curves and the difference in the binding energy of alphas and protons. However, a small correction has been applied to $\langle E_{EV} \rangle$ to account for the alpha and deuteron contamination by the use of the experimental data on $\pi^-$ absorption stars in emulsion.[11]

The knock-on prongs have been identified by the $g/g_0$ vs range method for those which ended while scattering measurements and other measurements were performed (See K-mesons). Almost all these particles were protons, with a few cases of K's and deuterons.

In Fig. 10 the spectrum of all nucleons is shown. This spectrum for $T_H > 10$ Mev can be described by the empirical relation:

$$\frac{d\langle N_H \rangle}{d T_H} = K T_H^{-a}$$

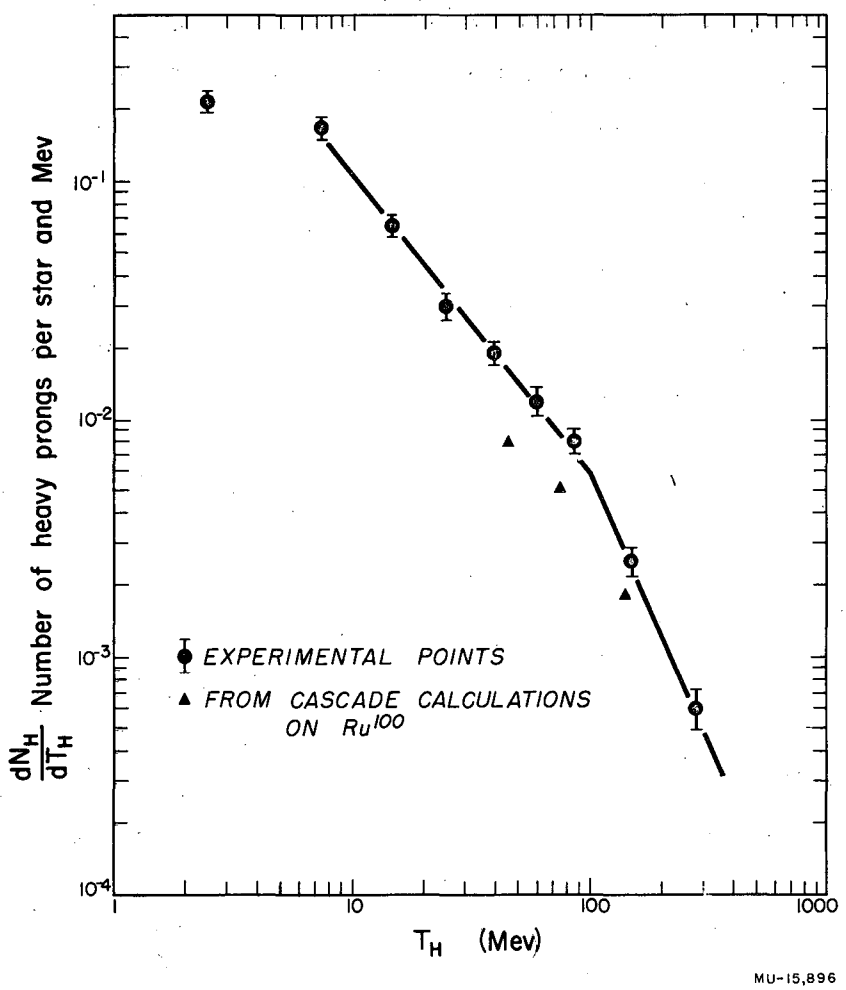


Fig. 10. The heavy-prong (proton) spectrum from antiproton-annihilation stars. The curve is an empirical fit to the data given in the text. The triangles are from cascade calculations on $Ru^{100}$ by Metropolis et al.[14]

where $\langle N_H \rangle$ is the average number of heavy prongs per star, $T_H$ the kinetic energy in Mev, and K and a are parameters: K = 2, a = 1.26 for 10 Mev < $T_H$ < 100 Mev, and K = 222, a = 2.28 for $T_H$ > 100 Mev. The shapes of the spectra for the stars at rest and in flight have been found to be similar, with only a difference in intensities such that: $K_{rest}/K_{flight} = \langle N_H \rangle_{rest} / \langle N_H \rangle_{flight}$. The discontinuity of the spectrum at about 7 Mev is a result of the influence of the Coulomb barrier against positive particle emission. An average Coulomb potential barrier of ~7 Mev is indicated. In the same figure, three points have been calculated by the use of the Monte Carlo calculations[12] on $\pi^-$, $\pi^+$ interactions with $Ru^{100}$ suitably averaged over the pion spectrum. Considering the large number of assumptions involved in these calculations and in their averaging over our pion spectrum, the comparison between these points and the experimental ones shows satisfactory agreement.

In Fig. 11 the number of stars as a function of $N_H$ ($N_H = N_{EV} + N_{KO}$) are plotted for stars at rest and in flight. From these distributions the average multiplicities of heavy prongs per star $\langle N_H \rangle$ are obtained: $\langle N_H \rangle_{rest} = 3.33 \pm 0.34$, and $\langle N_H \rangle_{flight} = 5.09 \pm 0.60$.

In Fig. 12 the number of stars as a function of the total energy given to the charged nucleons per star are shown for stars at rest and in flight. The total energy $E_H$ includes the kinetic energy together with 8-Mev binding energy. An average energy per star given to charged nucleons, $\langle \Sigma E_H \rangle_{rest} = 144 \pm 15$ Mev and $\langle \Sigma E_H \rangle_{flight}$ $220 \pm 26$ Mev, is then obtained.

The differences observed in $\langle \Sigma E_H \rangle$ and $\langle N_H \rangle$ for stars in flight and at rest have been attributed to a difference in the penetration of the antiprotons into the nucleus, resulting in a difference in the amount of pion interaction (see Section IV B, 1).

In Table IV a summary is given of the average number, total energy per star, and energy per prong for the evaporation, the knock-on, and the combined heavy prongs, as a function of the charged-pion multiplicity and for stars at rest, in flight, and combined. From this table one can observe that (a) the number of heavy prongs decreases

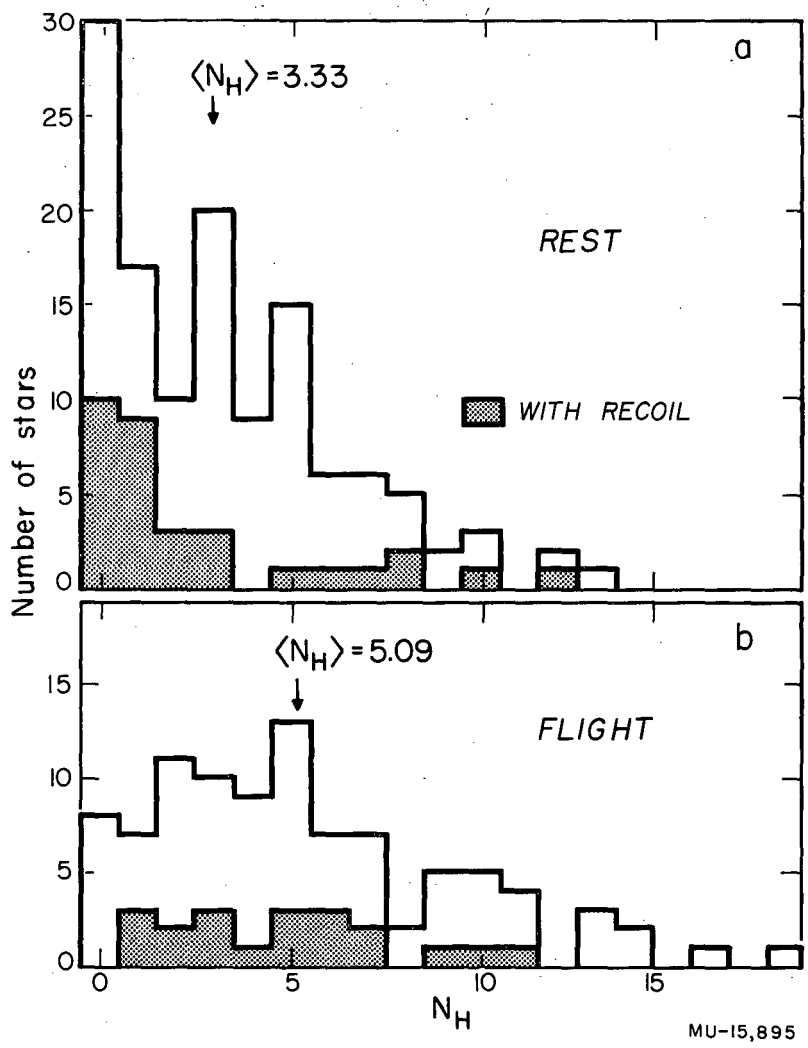


Fig. 11. The heavy-prong distribution from antiproton-annihilation stars.

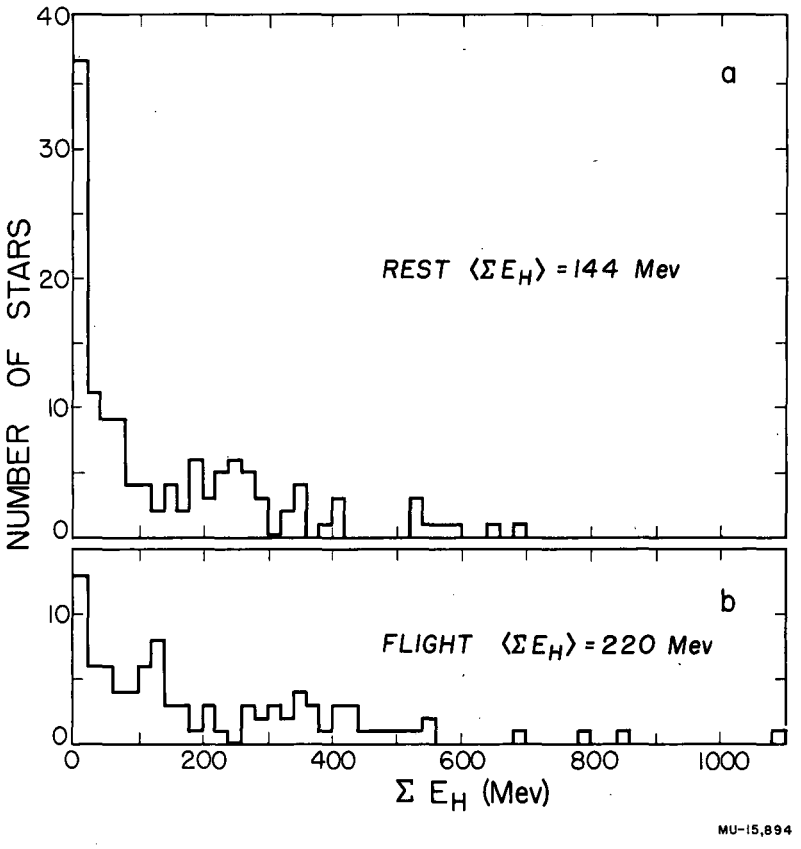


Fig. 12. The distribution of the energy emitted in heavy prongs (protons) per antiproton-annihilation star.

Table IV

The average values for the number of heavy prongs, the energy per heavy prong, and the energy in heavy prongs per star.

| Interaction | $N_\pi \pm$ | No. of stars | No. of heavy prongs | | | Energies (Mev)[a] | | | | | |
|---|---|---|---|---|---|---|---|---|---|---|---|
| | | | | | | Per prong | | | Per star | | |
| | | | $\langle N_{EV} \rangle$ | $\langle N_{KO} \rangle$ | $\langle N_H \rangle$ | $\langle E_{EV} \rangle$[b] | $\langle E_{KO} \rangle$ | $\langle E_H \rangle$ | $\langle \Sigma E_{EV} \rangle$[b] | $\langle \Sigma E_{KO} \rangle$ | $\langle \Sigma E_H \rangle$ |
| At rest | 0-2[d] | 56 | 2.8 | 1.3 | 4.1 | 17.1 | 109.5 | 45.5 | 48.4 | 136.8 | 185.2 |
| | 3 | 32 | 2.1 | 0.9 | 3.0 | 16.8 | 98.8 | 43.0 | 34.7 | 95.7 | 130.4 |
| | 4-6 | 25 | 1.4 | 0.4 | 1.8 | 15.1 | 121.2 | 39.2 | 20.4 | 48.5 | 68.9 |
| | 0-6 | 126[c] | 2.30 | 1.03 | 3.33 | 17.0 | 103.0 | 43.4 | 39.1 | 105.4 | 144.5 |
| In flight | 0-2[d] | 45 | 4.8 | 2.1 | 6.9 | 17.3 | 108.2 | 43.5 | 83.2 | 216.8 | 300.0 |
| | 3 | 30 | 3.3 | 1.2 | 4.5 | 16.3 | 105.1 | 39.6 | 54.4 | 126.1 | 180.5 |
| | 4-6 | 11 | 1.2 | 0.7 | 1.9 | 15.8 | 82.5 | 41.2 | 18.7 | 60.0 | 78.7 |
| | 0-6 | 95[c] | 3.55 | 1.54 | 5.09 | 18.0 | 101.8 | 43.3 | 63.9 | 156.4 | 220.3 |
| All combined | 0-2[d] | 101 | 3.7 | 1.6 | 5.3 | 17.2 | 108.9 | 44.6 | 63.9 | 172.4 | 236.3 |
| | 3 | 62 | 2.7 | 1.1 | 3.8 | 16.6 | 101.8 | 41.4 | 44.2 | 110.4 | 154.6 |
| | 4-6 | 36 | 1.3 | 0.5 | 1.8 | 15.3 | 109.4 | 39.8 | 19.9 | 52.0 | 71.9 |
| | 0-6 | 221[c] | 2.83 | 1.24 | 4.07 | 17.4 | 102.5 | 43.4 | 49.5 | 126.9 | 176.4 |

[a] These energies include a binding energy of 8 Mev per prong.

[b] The energies were assigned on the assumption that all prongs were protons. Actually deuterons and alpha particles are also present, and a correction for this effect is made later.

[c] These numbers include the events occurring near the surface of the emulsion ($\Delta Z < 20\ \mu$), for which no pion multiplicity was assigned.

[d] No $\bar{P}_\rho$ events have been included. These amount to $2\ ^{+3}_{-2}$ % of all stars at rest.

with $N_{\pi}\pm$ (b) the average energies $\langle E_{EV} \rangle$ and $\langle E_{KO} \rangle$ are independent of $N_{\pi}\pm$ and of whether the stars are in flight or at rest. The strong dependence of $\langle N_H \rangle$ on $N_{\pi}\pm$ indicates that pion absorption is the main channel of energy given to the nucleus. The constancy of $\langle E_{EV} \rangle$ and $\langle E_{KO} \rangle$ can be understood as follows: The knock-on prongs mainly come from pion absorption and direct collisions of the pions with the nucleons. But these processes depend only upon the pion spectrum which is about the same for stars in flight and at rest and for the different $N_{\pi}\pm$ values. The evaporation prongs are understood to be products of the "evaporation" of the nucleus through its potential barrier.[13] The spectrum of the evaporation prongs does not vary much with the variation of the excitation energy, being rather a characteristic of the nuclear-potential depth.

# IV. DISCUSSION

## A. The Annihilation Process and Best-Fit Values

An analysis of the annihilation stars in nuclear emulsion is attempted in this section. The analysis is based on the fact that the antiproton annihilates with one nucleon in the center-of-mass system, transforming the available energy mainly into π mesons. The pions being produced inside the nucleus interact with the nucleus before they escape.

In Fig. 13a diagrammatic representation of the annihilation process, subsequent phenomena, and related quantities are shown. The $\bar{P}$-nucleon system having an available energy $W = 2mc^2 + T_{\bar{P}}$ transforms into an average pion multiplicity $\langle N_\pi \rangle$ (the discussion is limited only to pions because K mesons are very rare and they will give only a small correction to the analysis). Here $T_{\bar{P}}$ is the antiproton kinetic energy and B is the small (~8 Mev) binding energy of the nucleon. These pions have an average energy $(E'_\pi)$. An energy balance in this stage of the process gives:

$$\langle N_\pi \rangle = \frac{W - \langle \Sigma E_{K-\bar{K}} \rangle}{\langle E'_\pi \rangle}, \qquad (1)$$

where $(\Sigma E_{K-\bar{K}})$ is the average energy per star given to K mesons.

On their way out of the nucleus, the pions give rise to pion interactions with the rest of the nucleus. If the average number of interacting pions (per star) is denoted by $\nu$ and if a is the fraction absorbed, then $\nu a$ pions will not come out of the nucleus. Thus, the pion multiplicity after the pions have left the nucleus is $(N_\pi - a\nu)$. Out of these, only charged pions can be observed and with an efficiency $\epsilon$. Let $(\pi^{\pm 0}/\pi^{\pm})$ be the ratio of all pions to the charged ones and $\langle N_{\pi^\pm} \rangle$ the observed pion multiplicity, then the following relation is obtained:

$$\langle N_\pi \rangle = \epsilon^{-1} \left( \frac{\pi^{\pm 0}}{\pi^{\pm}} \right) \langle N_{\pi^\pm} \rangle + a\nu \,. \qquad (2)$$

The average observed pion energy $(\bar{E}_\pi)$ differs from the primary energy $(E'_\pi)$ by the effects of the inelastic scattering, the energy

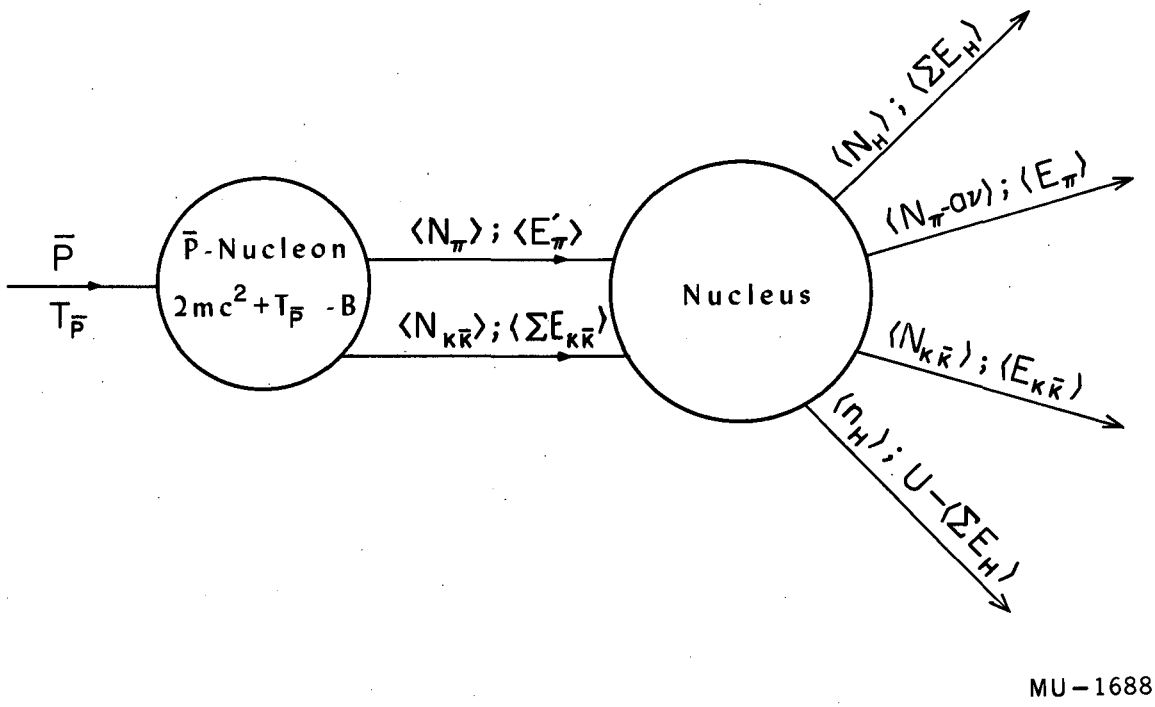


**Fig. 13.** A diagrammatic presentation of the annihilation process in complex nuclei.

dependence of the pion absorption, and finally by the influence of the pion nuclear potential $V_\pi$. The effects of pion interaction decrease the pion energy. The average pion energy after pions have interacted is $(E'_\pi - w)$, where w has been computed from the energy dependence of the pion interaction (Fig. 14) averaged over the pion spectrum. If $E_0$ is the average pion energy after the inelastic scattering, we have

$$\langle E_\pi \rangle = \frac{\left(\langle E'_\pi \rangle - w\right)\left(\langle N_\pi \rangle - \nu\right) + (1-\hat{a})\nu E_0}{\langle N_\pi \rangle - \hat{a}\nu} - V_\pi . \quad (3)$$

The energy U lost by the pions escaping the nucleus is given to the nucleus. The nucleus being left in a rather highly excited state releases this energy mainly through nucleon emission. If $\langle E'_\pi \rangle + w_0$ is the average energy of the interacting pions where $w_0$ has been computed from the energy dependence of the pion interaction (Fig. 14),[4] we then have

$$U = \nu \left\{ \langle E'_\pi \rangle + w_0 - (1-a) E_0 \right\} + V_\pi \left( \langle N_\pi \rangle - a\nu \right). \quad (4)$$

An average energy per star $\langle \Sigma E_H \rangle$ is observed to be released by the charged nuclear prongs of multiplicity $\langle N_H \rangle$, mainly protons. The remaining energy $U - \langle \Sigma E_H \rangle$ is assumed to be released by neutral particles, mainly neutrons. From other studies of $\pi$ meson interactions in photographic emulsion and Monte Carlo calculations of the same problem, empirical relations can be established for the branching ratios in the multiplicity and the energy given to the charged and the neutral nuclear particles. These are

$$\nu = \langle N_H \rangle / n_H \quad (5)$$

and

$$U = h \langle \Sigma E_H \rangle, \quad (6)$$

where $n_H$ (average number of heavy prongs per nonelastic pion interaction) and h are empirical constants.[4]

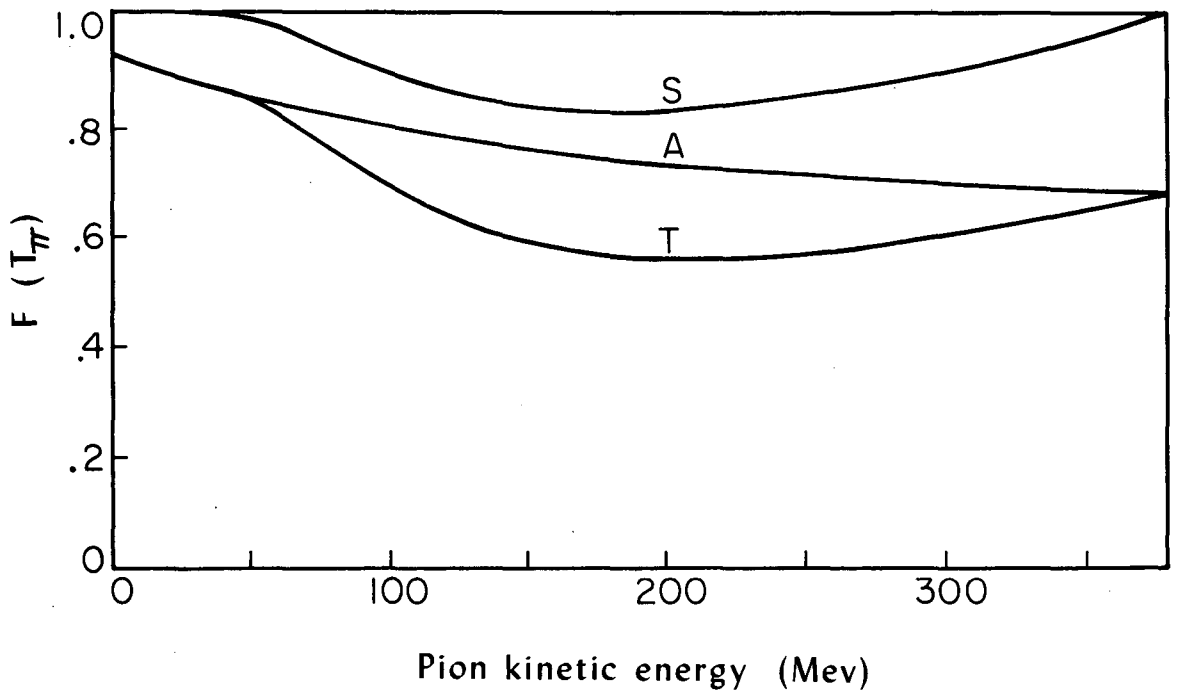


MU-16884

Fig. 14. Calculation of the fraction of noninteracting pions as a function of energy, for annihilations occurring at R'. (S) denotes not scattered inelastically, (A) not absorbed, and (T) not inelastically scattered or absorbed.

Equations (1) to (6), except (2), were solved for the four quantities $\langle E'_\pi \rangle$, $\langle N_\pi \rangle$, $\nu$, and U by successive approximations since the system is overdetermined. In this particular solution the pion potential $V_\pi = 0$ was assumed. The values of the other quantities in these equations have been tabulated in Table V together with their definition and the source of their numerical value. The analysis has been carried out separately for stars in flight and at rest. These derived quantities are the "best-fit values", and the errors assigned to them do not reflect any systematic errors inherent in the analysis we made but reflect only the errors assigned to the "input" quantities.

Using the best-fit values of $\langle N_\pi \rangle$ and $\nu$ in Eq. (2) we have obtained the value of $\epsilon^{-1}(\pi^{\pm 0}/\pi^{\pm})$. We note that it is not possible to calculate either $\epsilon$ or $(\pi^{\pm 0}/\pi^{\pm})$ separately because they occur as a product. However, with an estimated value $\epsilon = 0.90 \pm .05$, we obtain $(\pi^{\pm 0}/\pi^{\pm}) = 1.56 \pm 0.16$, which is in good agreement with charge independence requiring $(\pi^{\pm 0}/\pi^{\pm}) = 3/2$. This result leaves little room for other neutral particles present in the annihilation process or for violation of the charge-independence principle. (It should be noted that neutrons have been taken into account in U and $K^0$ or $\bar{K}^0$ mesons in $\langle \Sigma E_{K\bar{K}} \rangle$).

We will make a criticism of the previous analysis based on the pion multiplicity $\langle N_\pi \rangle$. We will accept the measured pion multiplicity with the hydrogen[14] and propane[10] bubble chambers experiments as the true one. From these experiments we have $\langle N_\pi \rangle_H = 4.8 \pm 0.3$, while our work predicts $(N_\pi)_{Em} = 5.35 \pm 0.28$. In the chamber work, $\langle N_\pi \rangle_H$ was deduced from Eq. (2), where no pion absorption took place, the pion detection efficiency was 1, and the observed $\langle N_{\pi^\pm} \rangle$ was used. In this work the multiplicity came out mainly from the pion energy $(E'_\pi)$.

The difference between $\langle N_\pi \rangle_H$ and $\langle N_\pi \rangle_{Em}$, though not statistically significant, may still be real because of any one or a combination of the following effects:

(a) There might be a remaining systematic error in $\langle E'_\pi \rangle$ from distortion in the plates, giving a lower energy for the pions for which scattering measurements were performed.

Table V

Definition of the quantities used in Eqs. (1)-(6) together with their numerical values, errors, and sources.

| Symbol | Definition | At rest | In flight | Combined | Source |
|---|---|---|---|---|---|
| A. Input Data from This Experiment | | | | | |
| $\langle W \rangle$ | Average total energy available per star in annihilation (Mev) | 1868 | 2009 | 1927 | Dirac theory and measurement of $\bar{p}$ kinetic energy |
| $\langle E_\pi \rangle$ | Average total pion energy (Mev) | 324±21 | 361±30 | 339±18 | Direct measurements with estimated ($\sim 5\%$) corrections |
| $\langle \Sigma E_H \rangle$ | Average energy per star used for heavy-prong (proton) emission (Mev) | 144.5±15 | 220.3±26 | 176.4±13 | Direct measurements, considering heavy prongs as protons |
| $\langle \Sigma E_{K\bar{K}} \rangle$ | Average total energy used per star for $K\bar{K}$ pair production (Mev) | 50±25 | 50±25 | 50±25 | Direct measurements and estimates |
| $\langle N_H \rangle$ | Average number of heavy prongs per star | 3.33±.34 | 5.09±.60 | 4.07±.31 | Direct measurements |
| $\langle N_{\pi^\pm} \rangle$ | Observed average charged-pion multiplicity | 2.50±.26 | 2.30±.28 | 2.41±.19 | Direct measurements |
| $\langle N_{\pi^\pm} \rangle_0$ | Observed average pion multiplicity for stars with $\Sigma E_H \lesssim 40$ Mev | 3.07±.45 | 3.35±1.0 | 3.15±.41 | Direct measurements |

Table V (cont'd)

| Symbol | Definition | Rest and flight combined | | | Source |
|---|---|---|---|---|---|
| B. Input Data from Pion Experiments and Calculations | | | | | |
| a | Fraction of interacting pions absorbed | ⟵ 0.75±.03 ⟶ | | | Estimated from pion-interaction experiments averaged over observed pion spectrum |
| $E_0$ | Average final total energy of inelastically scattered pions (Mev) | ⟵ 215±15 ⟶ | | | Estimated from pion-interaction experiments averaged over observed pion spectrum |
| $n_H$ | Average number of heavy prongs per nonelastic pion interaction | ⟵ 2.5±0.2 ⟶ | | | Estimated from pion-interaction experiments averaged over observed pion spectrum |
| h | Ratio of total energy given to nucleons to the total energy given to protons | ⟵ 2.7±.2 ⟶ | | | Estimated from evaporation theory and experiments and from calculations on pion-initiated cascades |
| w | Energy correction term due to pion interactions (Mev) | 5±2 | 8 ± 3 | 6±2 | Auxiliary quantity based on observed pion spectrum and pion m.f.p. in nuclear matter. |
| $w_0$ | Energy correction term due to pion interactions related to w by $w_0=w(\langle N_\pi \rangle - \nu)/\nu$ (Mev) | 15±6 | 13±5 | 14±5 | Auxiliary quantity based on observed pion spectrum and pion m.f.p. in nuclear matter. |

Table V (cont'd)

| Symbol | Definition | At rest | In flight | Combined | Source |
|---|---|---|---|---|---|
| C. Derived Quantities | | | | | |
| $\langle E'_\pi \rangle$ | Average primary total pion energy (Mev) | 337±21 | 367±25 | 350±18 | Best-fit evaluation of Eqs. (1)-(6) |
| U | Average energy per star used for proton and neutron emission (Mev) | 393±36 | 612±45 | 491±37 | Best-fit evaluation of Eqs. (1)-(6) |
| $\langle N_\pi \rangle$ | Average pion multiplicity | 5.39±34 | 5.33±40 | 5.36±28 | Best-fit evaluation of Eqs. (1)-(6) |
| $\nu$ | Average number of interacting pions | 1.32±.14 | 1.93±.14 | 1.61±.12 | Best-fit evaluation of Eqs. (1)-(6) |
| $\epsilon^{-1}(\pi^{\pm o}/\pi^{\pm})$ | $\epsilon^{-1}$ is the efficiency correction factor. $(\pi^{\pm o}/\pi^{\pm})$ is the average ratio of all pions to the number of charged pions | 1.76±.23 | 1.69±.27 | 1.72±.18 | Best-fit evaluation of Eqs. (1)-(6) |

(b) We have assumed $V_\pi = 0$, which is not well justified. The pion potential is energy-dependent [15] and it is closely related to the shape of the nucleon distribution in the nucleus. At low pion energies, $V_\pi$ is of the order of 30 to 35 Mev, decreases with increasing energy, passes through zero at the (3/2, 3/2) pion-nucleon resonance, and becomes negative above this resonance. [15] Because of this peculiar energy dependence of the pion potential and the fact that antiprotons annihilate at the surface of the nucleus, the over-all effect of the potential might average to zero when averaged over the entire pion spectrum. The effect of the pion potential, might, however, be significant, and the simplification $V_\pi = 0$ reflects the rather crude knowledge existing on this matter.

(c) The energy-momentum relation for pions is not the same in free space as in the nucleus. [16] This certainly changes the phase space of the pions in the final state of the annihilation. This difference may be significant, and thus the multiplicity of $\bar{P}$-nucleon annihilations could be inherently different. This argument is independent of the model used for the annihilation if the matrix element of the annihilation is the same in both cases. [17]

In the analysis, secondary-pion production by pion-nucleon interaction has been neglected. An overestimate of this effect decreases $\langle N_\pi \rangle$ by 1.5% which is insignificant. This estimate was deduced on the assumption that 5% of the interacting pions give rise to pion production. [18]

The pion multiplicity can be obtained from less "obscure" arguments if we consider only the stars with $E_H \leqslant 40$ Mev and assume that in those stars no pion absorption took place. This gives a lower limit for the pion multiplicity. With conservation of charge independence assumed, and an estimated value of $\epsilon = 0.90 \pm 0.05$, [4] from Eq. (2) we get for these stars $\langle N_\pi \rangle \geq 5.2 \pm 0.7$. The result, although statistically insignificant, is again higher than the multiplicity found in the hydrogen- and propane-bubble-chamber experiments.

## B. Amount of Pion Interaction

### 1. The Radius of Annihilation

In this section we will attempt to make a calculation of the amount of pion interaction produced in the annihilation process in complex nuclei. A pion is considered to have interacted with the nucleus if it has been absorbed or inelastically scattered. From this calculation and the "observed" amount of pion interaction, we will be able, first, to find the average radius of annihilation and, second, to find the cross section for antiproton-nucleon annihilation for a given shape of the nucleus.

Consider that the shape of the nucleus is described by a Fermi-like spherical distribution:

$$\rho(r) = \rho_0 \left\{ 1 + e^{\frac{r-R}{a}} \right\}^{-1}, \tag{7}$$

where $R = r_0 A^{1/3}$, $a = 0.5 \times 10^{-13}$ cm, $r_0 = 1.07 \times 10^{-13}$ cm, A is the atomic number of the nucleus, and $\rho_0$ is defined through the normalization condition $\int_{\infty} \rho(r) d^3\vec{r} = A$. This leads to

$$\rho_0 = 3A/4\pi R(R^2 + \pi^2 a^2). \tag{8}$$

Let $r_a$ be the distance of annihilation from the center of the nucleus, and assume that the pions emitted from the point of annihilation are isotropically distributed in the laboratory system. This is a reasonably good assumption as can be seen from Fig. 8. Let us consider an orthogonal system with its origin at the center of the nucleus and with the z axis passing through the annihilation point. Furthermore, let $\theta$ be the angle between the direction of emission of a pion with the z axis and $\phi$ the angle of projection of the direction of emission of a pion on the xy plane with respect to the x axis. The pion will "see" m nucleons/cm$^2$ from the production point,

$$m(\theta) = \int_0^{\infty} \rho(r)\, ds, \tag{9}$$

where s is taken along the line of the pion's motion.

If $\lambda(E_\pi)$ is the mean free path in nucleons/cm$^2$ for pion interaction, and $E$ is the pion energy, then $e^{\frac{-m(\theta)}{\lambda(E_\pi)}}$ is the probability for the pion to emerge from the nucleus without interaction. If we average over all pion directions, then the fraction $F(E_\pi)$ of pions which does not interact is given by:

$$F(E_\pi) = \frac{1}{4\pi} \int_0^{2\pi} d\phi \int_{-1}^{1} e^{\frac{-m(\theta)}{\lambda(E_\pi)}} \, d\cos\theta. \qquad (10)$$

Now it is possible to integrate Eq. (10) over $\phi$ because of the spherical symmetry of the nucleon distribution in the nucleus:

$$f(E_\pi) = \frac{1}{2} \int_{-1}^{1} e^{\frac{-m(\theta)}{\lambda(E_\pi)}} \, d\cos\theta. \qquad (11)$$

To simplify the mathematical difficulties involved in the integration of Eqs. (9) and (11), we have assumed a nucleus of uniform density $\rho_0$. The radius of this uniform nucleus is denoted by R', which turns out to be a little larger than R, $R'/R = (3/4\pi r_0^3 \rho_0)^{1/3}$. Under this assumption, Eq. (11) can be integrated for specific values of the annihilation radius $r_a$:

(a) If the annihilation occurs inside this uniform nucleus and if the probability for annihilation is proportional to the volume ($\langle r_a \rangle = 3R'/4$), then we have[19]

$$F(E_\pi) = 3\left\{\frac{1}{2x} - \frac{1}{x^3} + \frac{1}{x^3}(1+x)e^{-x}\right\} \qquad (12)$$

where $x(E_\pi) \equiv 2R'\rho_0/\lambda(E_\pi)$.

(b) If the annihilation occurs on the surface of the sphere ($r_a = R'$), then we have[20]

$$F(E_\pi) = \frac{1}{2}\left[1 + (1 - e^{-x})/x\right]. \qquad (13)$$

(c) For pion production outside the sphere ($r_a \gg R'$), we have used the approximate formula

$$F(E_\pi) \simeq \frac{1}{2}\left[1 + \sqrt{1 - \left(\frac{R'}{2a}\right)^2} + \frac{2}{2n_0\rho_0}\left(1 - \sqrt{1 - \left(\frac{R'}{2a}\right)^2}\right)(1 - e^{-x})\right]. \qquad (14)$$

We have calculated $F(E_\pi)$ as a function of energy, using mean free paths given by Frank, Gammel and Watson[15] and using a proper average over the emulsion $\langle A \rangle = 67$. In Fig. 14 we show $F(E_\pi)$ as a function of energy as it has been calculated from Eq. 13. Curve (T) represents the fraction of pions which did not interact ($F_T$) and has been calculated by the use of the total mean free path.[15] Curve A represents the fraction of pions which was not absorbed ($F_A$) and was calculated by the use of the absorption mean free path.[15] By subtraction of $F_A$ from $F_T$, the fraction of pions that do not undergo inelastic scattering has been obtained (Curve S). As we will see in this section, the antiprotons annihilate at an average distance from the center of the nucleus $r_a \sim R'$. For this reason, we have used the energy dependence of $F_S(E_\pi)$ and $F_A(E_\pi)$ and the values $\nu$, a, and b of Table V to calculate the correction terms w and $w_0$ discussed in Section IVA and Table V.

Similar calculations of $F(E_\pi)$ have been performed by the use of Eqs. 12, 14 for $r_a = 1.1R'$, $1.2R'$, $1.3R'$, $1.4R'$. From the calculations of $F(E_\pi)$ at $r_a/R' = 3/4$, 1, 1.1, 1.2, 1.3, and 1.4, the average $\overline{F}$ over the pion spectrum has been obtained for each radial distance. In Fig. 15a the fraction of pion interaction, $1-\overline{F}$, is plotted as a function of the radius of annihilation, $r_a$, normalized to the half-density radius, R.

The same calculations have been carried out by varying $r_0$ from $1.0 \times 10^{-13}$ cm to $1.4 \times 10^{-13}$ cm and separately for light and heavy nuclei. The calculations show that the amount of pion interaction is not sensitive to $r_0$. A dependence on A is present; it is not very large, however, and the averaging over the emulsion nuclei is not critical. The dependence on a is expected to be much smaller than the dependence on $r_0$, and it has not been considered. [This can be seen from the dependence of $\rho_0$ on $r_0$ and a through Eq. (7)]

In this calculation the approximation of the nucleus to be of uniform density is not a very accurate one because of the small mean free path for pion interaction. This simplification of the nuclear shape gives less pion interaction than the realistic case described by $\rho(r)$. The difference between them increases with $r_a/R$ and approaches zero

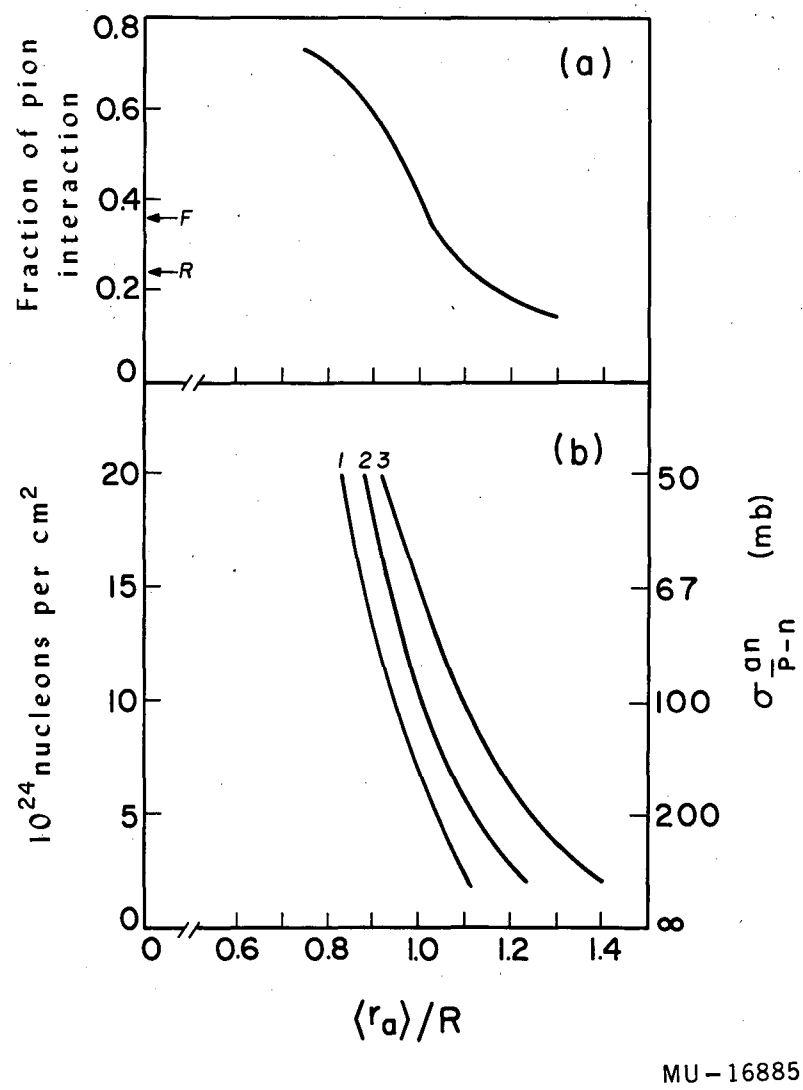


Fig. 15. (a) The percentage of interacting pions as a function of the average annihilation radius. The arrows marked R and F represent the percentage of interacting pions computed for stars at rest and in flight, respectively.

(b) The average depth of antiproton penetration into the nucleus as a function of the annihilation radius. Both curves are expressed in units of R, the half-density radius.

as $r_a/R$ goes to zero. Because this discussion is rather exploratory, the approximation suffices.

The really difficult question in this problem is how well do we know the mean free path in nuclear matter. At present certain theoretical values are available,[15, 21] and there are large uncertainties in these calculations, especially near the (3/2, 3/2) resonance, which is very close to the average pion energy of the annihilation process.

Taking the results of the previous calculations seriously and using the best-fit values for the amount of pion interaction ($\nu/N_\pi$) from Table V, we expect average radii of annihilation for stars in flight and at rest to be $(r_a/R)_{flight} = 1.02 \pm 0.02$ and $(r_a/R)_{rest} = 1.10 \pm 0.02$. The errors correspond only to the statistical errors in the amount of pion interaction. From these results we see that the stars in flight occur deeper in the nucleus than ones at rest. The interpretation of this difference has been that the antiprotons, interacting in flight, go directly to the nucleus, while the ones at rest are captured into Bohr orbits.[4, 22] In addition, for the average element in emulsion already at the F and D energy levels, the antiprotons get annihilated because of the overlapping of these states with the nucleus and of the high value of the annihilation cross-section.

2. A Possible Investigation of the Surface of the Nucleus

It is shown here that the knowledge of average radius for antiproton annihilations in flight can give information on the nucleon distribution in the nucleus and in particular of the nuclear density at the "fringe" of the nucleus. This is a consequence of the large annihilation cross-section which causes the annihilation of the antiprotons as soon as they come close to nuclear matter.

Let b be the impact parameter of the antiproton relative to the center of the nucleus and $r_a$ the annihilation radius. The forward peaked $\bar{P}$-nucleon scattering cross section[23] and the application of the Pauli Principle on the scattered nucleon decreases the antiproton scattering in the nucleus substantially and, to a good approximation, it can be neglected. Let x be the coordinate of the antiproton on its linear path of motion. The inverse of the number of nucleons per $cm^2$

crossed by the antiproton up to the point of annihilation defines the elementary annihilation cross section with the nucleus:

$$\frac{1}{\sigma^{an}_{\bar{p}\text{-}n}} = \int_{\infty}^{r_a(b)} \rho'(r)dx. \qquad (15)$$

Here $\rho'(r)$ is a modification of the nuclear density $\rho(r)$ taking into account the finite range of the antiproton interactions. The connection between $\rho'(r)$ and $\rho(r)$ is given by:[24]

$$\rho'(r) = \int F(|\vec{r}-\vec{r}'|)\, \rho(r')d^3\vec{r}', \qquad (16)$$

where $f(|\vec{r}-\vec{r}'|)$ defines the strength of the annihilation interaction between an antiproton at the position $\vec{r}$, and a nucleon at $\vec{r}'$. In the case of local interactions we have $F(|\vec{r}-\vec{r}'|) \rightarrow \delta(\vec{r}-\vec{r}')$ and consequently $\rho'(r) \rightarrow \rho(r)$.

From Eq. (15) we have calculated $\sigma^{an}_{\bar{p}\text{-}n}$ as a function of the radius r for a given b, neglecting the effects of the nonlocal character of the interaction. For the exploratory nature of this work, this approximation suffices; in an accurate calculation, however, the effects of the nonlocality in the interaction must be considered.

In Fig. 15b the value of $\sigma^{an}_{\bar{p}\text{-}n}$ and its inverse are plotted as a function of the average annihilation radius for all antiproton impact parameters and the emulsion nuclei. We note that the averaging process over the emulsion nuclei is not very sensitive. The calculations have been made with $r_0 = 1.07 \times 10^{-13}$ cm and $a = 0.3 \times 10^{-13}$cm, $0.5 \times 10^{-13}$ cm, and $0.8 \times 10^{-13}$cm. If one uses the mean radius of annihilation for the stars in flight, found in the previous section for the three values of a, an elementary $\bar{P}$-nucleon cross section of 167mb, 106mb, and 50mb is obtained, respectively.

Considering that (a) antiproton scattering will be prevented if the scattered nucleon receives an energy less than 30 Mev--because of the Pauli Principle--, (b) the angular dependence of the scattering cross section is forward peaked,[23] and (c) the scattering cross section is equal to the annihilation cross section, a 5% decrease must be applied to $\sigma^{an}_{\bar{p}\text{-}n}$ to account for the scattering.[25] Thus for the Stanford

parameters of the nucleon distribution ($r_0 = 1.07 \times 10^{-13}$cm, a = $0.50 \times 10^{-13}$cm)[26] the predicted elementary annihilation cross section is $\sigma^{an}_{\bar{p}\text{-}n} = 100 \pm 12$ mb at an average laboratory antiproton kinetic energy of 140 Mev. The error quoted here is, again, the statistical one, and it does not reflect the reliability of the model. A comparison of the $\sigma^{an}_{\bar{p}\text{-}n}$ with the annihilation cross section in hydrogen gives a satisfactory agreement with $a = 0.5 \times 10^{-13}$cm,[23] while for $a = 0.3 \times 10^{-13}$cm and $0.8 \times 10^{-13}$cm the agreement is very poor.

Similar calculations can be performed for the stars at rest if Bohr orbits are assumed and the time of transition from higher to lower states is considered. This would afford additional information on the nuclear shape, but no calculations have been made. Some calculations for the states of $K^-$ mesons for the light and heavy emulsion elements have been made.[27]

## C. Aspects of the Statistical Model of Annihilation

### 1. General

It has become customary to compare the experimental results with the modified Fermi statistical theory of the annihilation process.[2,4] Modified means that the interaction volume of the Fermi theory is adjusted so that the calculated average pion multiplicity is equal to the observed one. In Table VI the distribution of pion multiplicity $P_n$ is given, neglecting K-$\bar{K}$ production, and considering energy-momentum conservation for the phase space used by Fermi,[28] and the Lorentz-invariant phase space[29] (see next section).

This modified Fermi statistical model gives a satisfactory agreement with the following experimental results:

(a) pion spectrum (Fig. 16),
(b) the charged-pion multiplicity $N_{\pi^\pm}$ (Fig. 17),
(c) the average pion energies as a function of $N_{\pi^\pm}$ (Table VII).

Table VI

Distribution of pion multiplicity $P_n$ according to the Fermi statistical model normalized for an interaction radius of $r = 2.5\hbar/m_\pi c$, for $\langle N_\pi \rangle = 5.4$.

| N | $P_n$ with Fermi phase space | $P_n$ with Lorentz-invariant phase space |
|---|---|---|
| 3 | 2.3 | 2.1 |
| 4 | 13.4 | 15.7 |
| 5 | 40.6 | 39.4 |
| 6 | 33.1 | 33.3 |
| 7 | 10.6 | 9.4 |

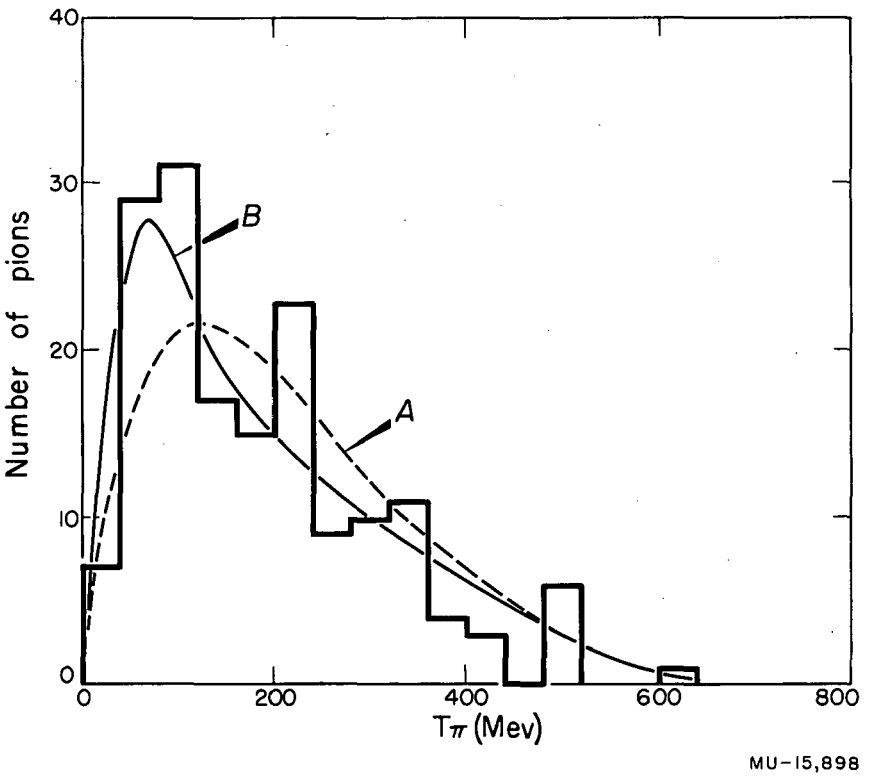


Fig. 16. The pion-energy spectrum. Curve A gives the pion-energy distribution as predicted by the normalized Fermi statistical model for $\langle N_\pi \rangle = 5.36$, and curve B gives this distribution corrected for the effects of pion absorption, inelastic scattering, and detection efficiency.

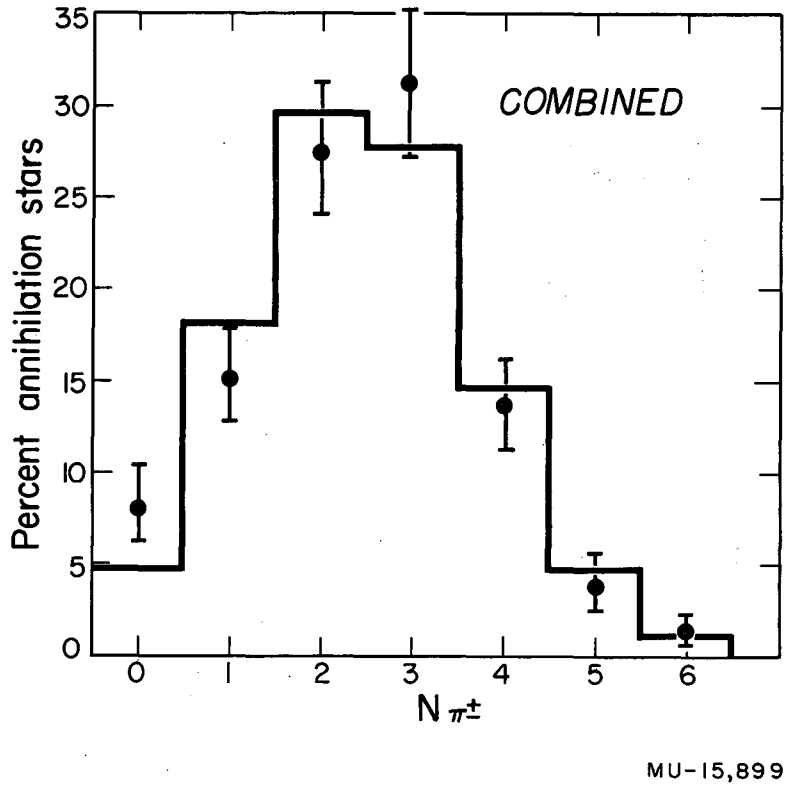


Fig. 17. The experimental charged-pion multiplicity distribution compared with the distribution of charged pions obtained from the normalized Fermi model for $\langle N_{\pi} \rangle = 5.36$, corrected for 32% loss through the effects of pion absorption and detection efficiency.

Table VII

The average experimental pion kinetic energy as a function of the observed charged-pion multiplicity. Also shown for comparison are the values computed from the normalized Fermi statistical model.

| | At rest | | | | In flight | | | | Combined | | | |
|---|---|---|---|---|---|---|---|---|---|---|---|---|
| $N_\pi \pm$ | No. of pions $\leq 15^\circ$ dip | $\langle T_\pi \rangle_{raw}$ (Mev) | $\langle T_\pi \rangle$ (Mev) | $\langle T_\pi \rangle_{Fermi}$ (Mev) | No. of pions $\leq 15^\circ$ dip | $\langle T_\pi \rangle_{raw}$ (Mev) | $\langle T_\pi \rangle$ (Mev) | $\langle T_\pi \rangle_{Fermi}$ (Mev) | No. of pions $\leq 15^\circ$ dip | $\langle T_\pi \rangle_{raw}$ (Mev) | $\langle T_\pi \rangle$ (Mev) | $\langle T_\pi \rangle_{Fermi}$ (Mev) |
| 1-2 | 31 | 194 | 211 | 220 | 13 | 294 | 301 | 230 | 44 | 220 | 237 ± 33 | 224 |
| 3 | 36 | 163 | 180 | 199 | 32 | 195 | 212 | 204 | 68 | 178 | 195 ± 27 | 201 |
| 4-6 | 26 | 158 | 175 | 170 | 12 | 155 | 172 | 179 | 38 | 152 | 169 ± 36 | 172 |
| 1-6 | 99[a] | 167 | 184 ± 21 | 195 | 65[a] | 204 | 221 ± 30 | 206 | 164[a] | 172 | 199 ± 18 | 200 |

[a] These numbers include some pions from events occurring near an emulsion interface for which no $N_\pi \pm$ value was assigned.

## 2. The Pion-Pion Angular Distribution

In an attempt to see if $\pi$-$\pi$ forces are present in the annihilation process we have examined the $\pi$-$\pi$ angular distribution. In present models of the annihilation process, the pions are confined for a short time of $\sim 10^{-24}$ sec in a volume where mutual interactions between them can occur. The presence of $\pi$-$\pi$ forces will impose some correlation between the emitted pions. In the case where no correlation between the pions is present, the pion-pion angular distribution should be isotropic. Take, for instance, the $n^{th}$ pion as defining the z axis, and the angle between the z axis and the $i^{th}$ pion to be $\theta$. Then the distribution of the $i^{th}$ pion within the angle $\theta$ and the $\theta + d\theta$ would be proportional to the solid angle $\sin\theta d\theta d\phi$ if no restriction on the direction of the $i^{th}$ pion was imposed by the $n^{th}$ one.

However, the observed distribution is anisotropic, favoring large angles $\theta$.(See Fig. 9.) We then conclude that the pions cannot be considered independent among themselves. We know that, besides any other possible correlations of which we might think, we must still consider momentum-energy conservation laws which constrain the freedom of the pionic system. With simplified assumptions we can see that the conservation of momentum and energy influences the pion-pion angular distribution in such a way as to describe qualitatively the observed angular distribution. Assume for example that the symmetric configuration of momenta $\vec{p}_1, \vec{p}_2, \ldots, \vec{p}_n$ is the most probable one, and furthermore, that the average $\langle\gamma\rangle$ and $\langle\theta\rangle$ (see definitions in III A,5) correspond to this state. Simple geometrical calculations then give a value for $\langle\theta\rangle$ of $120^\circ$, $109.5^\circ$, and $108^\circ$ for stars with multiplicities 3, 4, and 6, respectively. All these multiplicities give a $\gamma$ which is in qualitative agreement with the observed value.

It follows then that before we interpret the observed anisotropy in terms of pion-pion interactions, we must first calculate the effects of the conservation laws on this distribution. Since the distribution is a combination of all pion multiplicities and because other similar integral distributions (spectrum, the charged-pion multiplicity $N_{\pi^\pm}$, and the average pion energies as a function of $N_{\pi^\pm}$) can be made to agree quite

well with the statistical models by adjusting only the volume of interaction, it is expected that a statistical treatment of the problem for our experimental data is equally justified.

We have calculated the pion-pion angular distribution for a system of $n$ indistinguishable pions of mass $\mu$ and total energy $W$, whose distribution is determined by Fermi phase space alone. Because of its noninvariant character, the Fermi phase space represents great difficulties in the transformations from one system of variables to another. Thus, it is rather difficult to compute the pion-pion angular distribution in an exact way for this case.

In order to overcome these mathematical difficulties we have considered instead an invariant form of the phase space used in field theory. This is actually the expression obtained from the covariant S-matrix theory of Feynman[30] if it is assumed that the S-matrix element for the emission of $n$ pions is simply a constant, independent of the momenta or energies of the emitted pions. If this constant is taken to be $V^n$, then, for the calculation of the probabilities ($P_n$) of annihilation into $n$ pions, this form of phase space gives essentially the same results as that used by Fermi (see Table VI). It is reasonable to expect that these phase-space expressions should give quite closely the same angular correlations between the pions, especially since they differ only by a factor $\left( \prod_{i=1}^{n} \omega_i \right)$ which varies relatively little over the different configurations available for the $n$ pions.

If we assume, then, that the matrix element for the $\bar{P}$-nucleon absorption is constant, the covariant transition probability for this process will be

$$T_n = A \, \frac{G(I)}{n!} \cdot \frac{(\mu \Omega)^n}{(2\pi)^{3n}} \, F_n(W^2), \qquad (17)$$

where $A$ is a constant independent of $n$, and $G_n(I)$ is the isotopic-spin weight factor. Here $F_n(W^2)$ is the invariant form of phase space defined by

$$F_n(W^2) = \int \delta\left( \sum_{i=1}^{n} \omega_i - W \right) \delta\left( \sum_{i=1}^{n} \vec{p}_i \right) \prod_{i=1}^{n} \frac{d_3 \vec{p}_i}{\omega_i} \, , \qquad (18)$$

where $\omega_i$ is the relativistic energy of the pion with momentum $p_i$:

$$\omega_i = \sqrt{p_i^2 + \mu^2}. \tag{19}$$

Since in the transition probability $T_n$ only the phase space contains the energy- and momentum-conservation laws, we will consider the phase space neglecting normalizing constants. Thus $F_n(W^2)$ can be written as

$$F_n(W^2) = \int \frac{d_3\vec{p}_n}{\omega_n} \left[ \int \delta \left\{ \sum_{i=1}^{n-1} \omega_i - (W-\omega_n) \right\} \delta\left( \sum_{i=1}^{n-1} \vec{p}_i + \vec{p}_n \right) \prod_{i=1}^{n-1} \frac{d_3\vec{p}_i}{\omega_i} \right]. \tag{20}$$

The square bracket represents the phase space for the (n-1) pions with energy $(W-\omega_n)$ and total momentum $-\vec{p}_n$.

Let us evaluate this square bracket in the Lorentz system in which $\sum_{i=1}^{n-1} \vec{p}_i$ has the value $\sum_{i=1}^{n-1} \vec{p}_i' = 0$, and $\sum_{i=1}^{n-1} \omega_i$ has the value $\sum_{i=1}^{n-1} \omega_i = W'$. From Lorentz invariance, $(\sum_{i=1}^{n-1} \omega_i)^2 - (\sum_{i=1}^{n-1} \vec{p}_i)^2$ has the same value in all coordinate systems. Evaluating this in the system just defined and in the laboratory system gives

$$W'^2 = (W-\omega_n)^2 - p_n^2 = W^2 + \mu^2 - 2W\omega_n. \tag{21}$$

In the transformed system, because $\left( \frac{d_3\vec{p}}{\omega} \right)$ is invariant and has the same value in all Lorentz systems, the square bracket becomes

$$\left[ \int \delta\left( \sum_{i=1}^{n-1} \omega_i' - W' \right) \delta\left( \sum_{i=1}^{n-1} \vec{p}_i' \right) \prod_{i=1}^{n-1} \frac{d_3\vec{p}_i'}{\omega_i} \right],$$

which is just $F_{n-1}(W'^2)$, according to Eq. (18). Hence, we have

$$F_n(W^2) = 4\pi \int_{\mu}^{[W^2 - n(n-2)\mu^2]/2W} p_n \cdot d\omega_n \cdot F_{n-1}(W'^2). \tag{22}$$

The upper limit has been determined from

$$(W^2 + \mu^2 - 2W\omega_n)^{\frac{1}{2}} = (n-1)\mu.$$

The functions $F_n(W^2)$ can now be calculated successively by means of Eq. (22), starting from $F_2(W^2)$, e. g.,

$$F_2(W^2) = 2\pi\left(1 - \frac{4\mu^2}{W^2}\right)^{\frac{1}{2}},$$

$$F_3(W^2) = 4\pi(2\pi)\int_{\mu}^{\frac{W^2 - 3\mu^2}{2W}} p\,d\omega\left(1 - \frac{4\mu^2}{W'^2}\right)^{\frac{1}{2}}, \text{ etc.}$$

The functions $F_n(W^2)$ have been calculated in the IBM 650 for n = 2, 3, 4, and 5 as a function of $W^2$. The $F_n(W^2)$ are smooth functions of $W^2$, and they have been approximated to a second order polynomial. Similarly, from Eq. (18) we can get the distribution in the momenta of two pions:

$$\Phi_n(\vec{p}_1, \vec{p}_2) = \iint \frac{d_3\vec{p}_1}{\omega_i} \cdot \frac{d_3\vec{p}_2}{\omega_2}\left[\int\left\{\delta\sum_{i=3}^{n}\omega_i - (W - \omega_i - \omega_2)\right\}\times \delta\left(\sum_{i=3}^{n}\vec{p}_i + \vec{p}_1 + \vec{p}_2\right)\prod_{i=3}^{n}\frac{d_3\vec{p}_i}{\omega_i}\right]. \quad (23)$$

Transforming to the system in which $\sum_{i=3}^{n}\vec{p}_i$ becomes $\sum_{i=3}^{n}\vec{p}''_i = 0$, and $\sum_{i=3}^{n}\omega_i$ takes the value $\sum_{i=3}^{n}\omega'_i = W''$, we see that the square bracket represents $F_{n-2}(W''^2)$, where

$$W'^2 = (W - \omega_1 - \omega_2)^2 - (\vec{p}_1 + \vec{p}_2)^2 = W^2 + 2\mu^2 - 2W(\omega_1 + \omega_2) + 2(\omega_1\omega_2 - \vec{p}_1\cdot\vec{p}_2). \quad (24)$$

Now, we have $\left(\frac{d_3\vec{p}_1}{\omega_1} \cdot \frac{d_3\vec{p}_2}{\omega_2}\right) \equiv p_1 d\omega_1 d\phi_1 p_2 d\omega_2 d\phi_2 \sin\theta d\theta$,

where $\theta$ is the angle between the two pions, one of them defining the z axis. Hence we may write

$$\Phi_n = 4\pi^2\int_{\theta} d\cos\theta\left[\iint p_1 p_2 d\omega_1 d\omega_2 F_{n-2}(W''^2)\right]. \quad (25)$$

Thus the pion-pion angular distribution in cos $\theta$ is

$$\Phi_n(\cos\theta) \alpha \iint p_1 p_2 F_{n-2}(W''^2) d\omega_1 d\omega_2. \quad (26)$$

For given value of cos $\theta$, the integration over $\omega_1$ and $\omega_2$ proceeds over the area defined by the limitations $\omega_1 \geq \mu$, $\omega_2 \geq \mu$, and $W''^2 \geq (n-2)^2\mu^2$. The area defined by these limits increases to with increasing $\theta$ and decreasing n.

The double integrals in Eq. (26) have been calculated on the IBM 650 computer for n = 4, 5, 6, and 7 as a function of cos $\theta$. The calculated $\Phi$ (cos $\theta$) are shown in Fig. 18 normalized to the same number of pion pairs. In Table VIII the ratio $\gamma$ and the $\langle\theta\rangle$ are given as a function of the pion multiplicity. The expected influence of the conservation laws is very clear in these distributions, e.g. decreasing anisotropy with increasing pion multiplicity. The degrees of freedom in the system of n pions are (3n - 4), if momentum and energy are conserved. As the pion multiplicity increases, the four constraints become less important, the correlation between pions is looser, and therefore the distribution becomes more isotropic.

In order to compute the angular distribution that corresponds to the annihilation process, it is necessary to average over these distributions according to the probability ($P_n$) for annihilation into n pions. The probability ($P_n$) has been taken from calculations of the statistical models (see Table VI) in which an interaction volume has been used such that the calculated and observed multiplicities are equal.

Table VIII

Theoretical calculations for $\langle\theta\rangle$ and $\gamma$ as a function of the pion multiplicity, using a Lorentz-invariant phase space with energy-momentum conservation.

| $N_\pi$ | 4 | 5 | 6 | 7 |
|---|---|---|---|---|
| $\langle\theta\rangle$ | 109° | 103° | 100° | 96° |
| $\gamma$ | 2.0 | 1.9 | 1.7 | 1.5 |

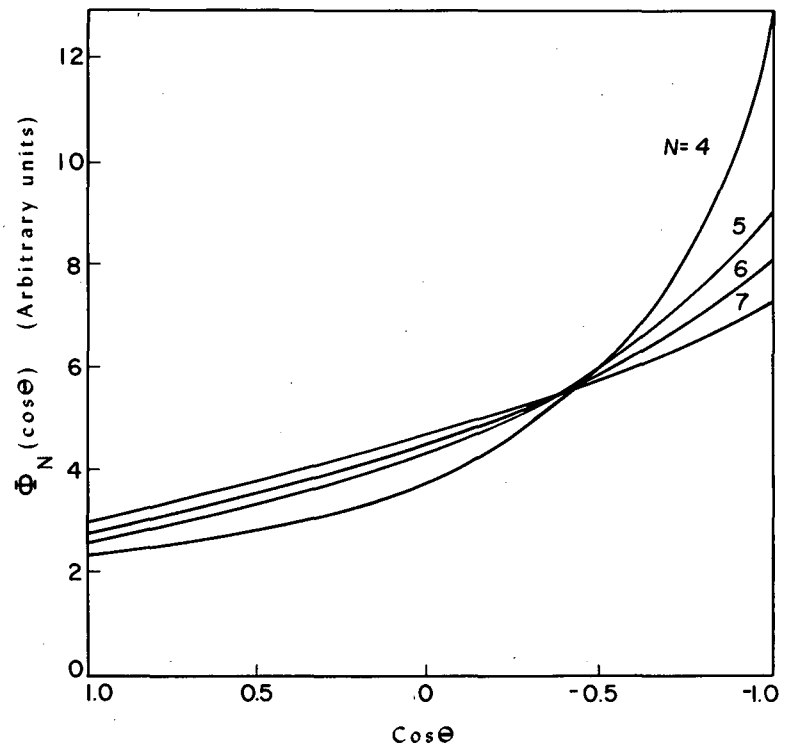


Fig. 18. Theoretical pion-pion angular distributions, using the statistical model of annihilation and Lorentz invariant phase space with conservation of energy and momentum.

It is expected that the use of the calculated $P_n$ will be as good as in the case of the pion spectrum, the charged-pion multiplicity $N_{\pi^\pm}$, and the average pion energies as a function of $N_{\pi^\pm}$, in which satisfactory agreement between theory and experiment were found. In addition the $\Phi_n(\cos\theta)$ has been weighted by $\frac{n(n-1)}{2}$ which represents the possible pion pairs in a star of multiplicity n. The distribution computed is plotted in Fig. 9 together with the experimental points. This distribution gives a ratio $(\gamma)_{calc} = 1.66$, and $\langle\theta\rangle_{calc} = 99.6^\circ$, while the observed values are: $(\gamma)_{obs} = 1.45 \pm 0.13$, and $\langle\theta\rangle_{obs} = 97 \pm 4^\circ$.

If one considers that scattering of pions in the nucleus reduces any anisotropy in pion angular distribution, the agreement between theory and experiment is striking. (A comparison of the pion-pion angular distribution for annihilations in emulsion and in hydrogen can show if there is any appreciable scattering of pions). If we assume that no appreciable amount of pions has been scattered in the nucleus (we have estimated 7% inelastic scattering) then the agreement is suggestive of the following:

(a) The observed anisotropy results from the conservation laws alone and gives no evidence for an influence of pion-pion interactions in the annihilation process.

(b) A statistical model of the annihilation process gives a good agreement with the integral distributions if an adjustment of the interaction volume is made.

(c) Independently of any assumptions, as for example charge independence, pion absorption, and efficiency of pion detection, the average pion multiplicity in the annihilation is larger than four.

## 3. On the K-Meson Spin

Sandweiss calculated the effects of the spin of the K meson on the abundance of K-$\bar{K}$ meson pairs in the annihilation process, assuming the Fermi statistical theory with conservation of energy, momentum, and angular momentum.[31] The spin of the K meson enters into the theory as a weight factor $(2S + 1)$ where S is the spin. We show

in Fig. 19 the results of his calculations together with the present $K\text{-}\bar{K}$ meson abundance. The $K\text{-}\bar{K}$ meson abundance favors a zero-spin K meson, but it is still to small to give meaningful agreement with the calculations. We think that, if possible, an application of the Sandweiss proposal to the Koba-Takeda model of the annihilation,[32] which decreases the $K\text{-}\bar{K}$ abundance, should be of interest.

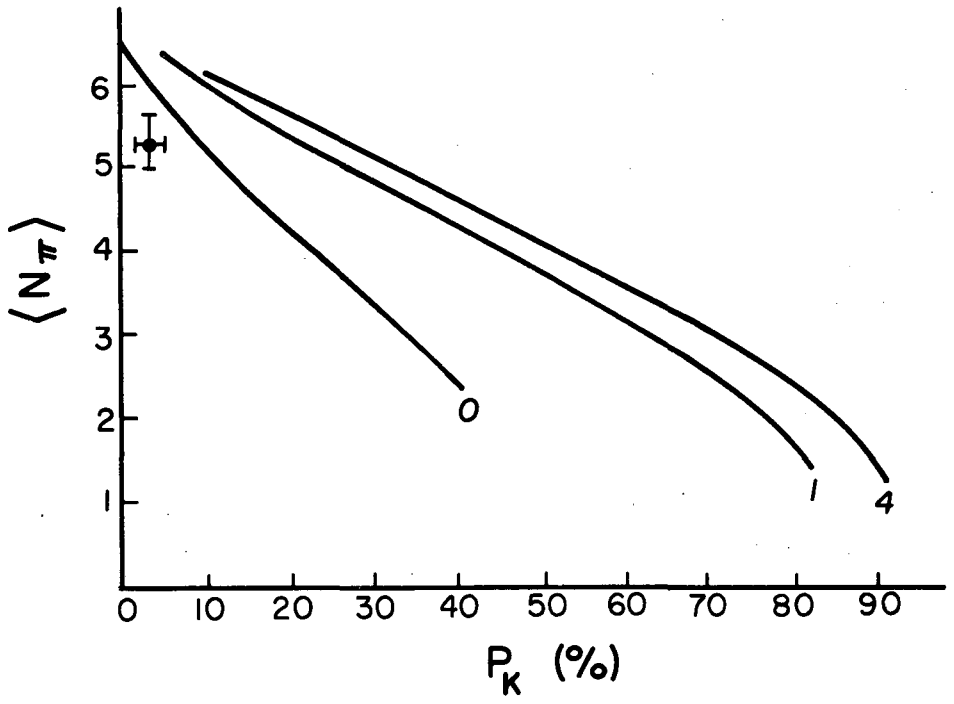


MU-16887

Fig. 19. The iso-spin lines for K-meson spin: 0, 1, 4.[30] $P_K$ is the abundance of K-$\bar{K}$ pairs as a function of $\langle N_\pi \rangle$.

## ACKNOWLEDGMENTS

I am grateful to Professor Gerson Goldhaber for his guidance, encouragement, and support throughout the course of this work. I am indebted to Professor Richard Dalitz who suggested to me the use of Lorentz-invariant phase space to deduce the pion-pion angular distribution and for many useful comments on this subject.

I am grateful to Professors Kenneth W. Watson, Charles Zemach, and Dr. Alfred E. Glassgold for many illuminating discussions on the problem of pion absorption. I am also grateful to Dr. Joseph Lepore for many discussions.

Many thanks are due to Mr. Rein Silberberg who as a partner in some of this work has made many contributions, especially in Table VII, in the computation of $w$ and $w_0$, and in multiple-scattering measurements. I am indebted to Mr. Lewis Agnew, Professor Owen Chamberlain, Dr. Louis Jauneau, and Professor Emilio Segrè for assistance in setting up the beam. I would like to express my thanks to each of the many scanners who have made possible this work with their conscientious effort. Finally, I want to thank my wife Naucikaa for her encouragement throughout my graduate studies and the typing of the papers.

This work was performed under the auspices of the United States Atomic Energy Commission.

BIBLIOGRAPHY

1. Chamberlain, Segrè, Wiegand, and Ypsilantis, Phys. Rev. 100, 947 (1955).
2. Chamberlain, Chupp, Ekspong, Goldhaber, Goldhaber, Lofgren, Segrè, Wiegand, Amaldi, Baroni, Castagnoli, Franzinetti, and Manfredini, Phys. Rev. 102, 921 (1956).
3. Goldhaber, Kalogeropoulos, and Silberberg, Phys. Rev., 110, 1474 (1958).
4. Chamberlain, Goldhaber, Jauneau, Kalogeropoulos, Segrè, and Silberberg, The Antiproton-Nucleon Annihilation Process. II, UCRL-8424 and Phys. Rev., in press.
5. Agnew, Chamberlain, Keller, Mermod, Rogers, Steiner, and Wiegand, Phys. Rev., 108, 1545 (1957).
6. T. D. Lee, Proceedings of the Seventh Annual Rochester Conference on High-Energy Nuclear Physics, (Interscience, New York, 1957) p. 12. He proposed that there may be left- and right-handed nucleons and consequently antinucleons, and that the one kind should not annihilate. This is not justified by this work because all antiprotons annihilate.
7. C. R. Weingart, Antineutron Production by Charge Exchange, Thesis, UCRL-8025, October, 1957.
8. Biswas, George, Peters, and Swamy, Nuovo cimento (Supp.) 12, 369 (1954).
9. E. Fermi and E. Teller, Phys. Rev. 72, 399 (1947).
10. Lander, Agnew, Elioff, Fower, Gilly, Oswald, Powell, Segrè, Steiner, White, Wiegand, and Ypsilantis, Bull. Am. Phys. Soc. 3, 402 (1958).
11. E. R. Marshak, Meson Physics (McGraw-Hill Book Co., New York, N. Y., 1952), pp. 180-190.
12. Metropolis, Bivins, Storm, Miller, Friedlander, and Turkevich, Phys. Rev. 110, 204 (1958).
13. J. M. Blatt and V. F. Weisskopf, Theoretical Nuclear Physics (Wiley and Sons, New York, 1952) pp. 340-379.
14. Horwitz, Miller, Murray, and Tripp, University of California Radiation Laboratory, private communication, 1959. Also report by O. Piccioni at the 1958 Geneva High-Energy Physics Conference.

15. Frank, Gammel, and Watson, Phys. Rev. 101, 891 (1956).
16. K. W. Watson, and C. Zemach, Nuovo Cimento 10, 452 (1958).
17. Charles Zemach, University of California, private communication, (1959).
18. At $T_{\pi}$ = 500 Mev, 1% charged-$\pi$-meson production was observed by Blau and Caulton, Phys. Rev. 96, 150 (1954), and 3% was computed by Metropolis et al., op. cit.
19. Brueckner, Serber, and Watson, Phys. Rev. 84, 258 (1951).
20. Webb, Iloff, Featherston, Chupp, Goldhaber, and Goldhaber, Nuovo cimento 8, 899 (1958).
21. There exist some experimental values on the interactions with Be, C, Cu, O, and Pb from 140 Mev to 400 Mev, and they are in good agreement with the theoretical calculations. See Ignatenko, Mukhin, Ozerov, and Pontecorvo, J. Exptl. Theoret. Phys U. S. S. R. 4, 351 (1957).
22. H. Bethe, and J. Hamilton, Nuovo cimento 4, 1 (1956).
23. Coombes, Cork, Galbraith, Lambertson, and Wenzel, Phys. Rev. 112, 1303 (1958).
24. Williams, R., Phys. Rev. 98, 1387 (1955).
25. Similar calculations have been made also by Jose Fulco, The Effective Mean Free Path of Antinucleons in Nuclear Matter. UCRL-8416 (1958).
26. Hofstader, Robert, Revs. Mod. Phys. 28, 214 (1956).
27. Chadwick et al., Cavendish Laboratory, England. From communication with D. J. Prowse, University of California at Los Angeles, California.
28. E. Fermi, Progr. Theoret. Phys. 5, 570 (1950).
29. Bipin Desai, Lawrence Radiation Laboratory, private communication.
30. Schweber, Bethe, and de Hoffmann, Mesons and Fields, Vol. I, (Row, Peterson and Co., Evanston, Ill., 1956), pp. 247-8.
31. Jack Sandweiss, (Thesis), On the Spin of K Mesons from the Analysi of Antiproton Annihilations in Nuclear Emulsions, UCRL-3577, October, 1956.
32. Z. Koba and G. Takeda, Progr. Theoret. Phys. 19, 269 (1958).